UC Riverside

UC Riverside Electronic Theses and Dissertations

Title

Synthesis and Characterization of Metal-Oxide Composite Materials for Permanent Magnetic Applications

Permalink

https://escholarship.org/uc/item/71h9j80g

Author

Volodchenkov, Aleksey

Publication Date

2012

Peer reviewed|Thesis/dissertation

eScholarship.org Powered by the California Digital Library
University of California

UNIVERSITY OF CALIFORNIA
RIVERSIDE

Synthesis and Characterization of Metal - Oxide Composite Materials for Permanent Magnetic Applications

A Thesis submitted in partial satisfaction
of the requirements for the degree of

Master of Science

in

Mechanical Engineering

by

Aleksey Volodchenkov

September 2012

Thesis Committee:
Dr. Javier Garay, Chairperson
Dr. Lorenzo Mangolini
Dr. Masaru Rao

Copyright by
Aleksey Volodchenkov
2012

The Thesis of Aleksey Volodchenkov is approved:

_____

_____

_____

Committee Chairperson

University of California, Riverside

Acknowledgements

Conducting research on bulk 3D composite materials has not been an easy feat. A lot of great mentoring was provided by my research advisor Dr. Javier E. Garay, associate professor in the Department of Mechanical Engineering at the University of California Riverside. Support was also offer by my lab mates, without whom, my study would have surely been less successful. Further encouragement was provided by my parents, Dmitriy Volodchenkov and Marina Volodchenkova, and brother Daniel Volodchenkov. Their constant support was responsible for my success. Lastly, a colossal amount of help was provided to me by my girlfriend Grissel Machuca. She understood the struggles of graduate school and always supported me. I am very appreciative of all those who have made my time in graduate school a success.

ABSTRACT OF THE THESIS

Synthesis and Characterization of Metal - Oxide Composite
Materials for Permanent Magnetic Applications

by

Aleksey Volodchenkov

Master of Science, Graduate Program in Mechanical Engineering
University of California, Riverside, September 2012
Dr. Javier E. Garay, Chairperson

State of the art magnets depend heavily on the use of rare-earth materials and cost 10 to 20 times more than other magnets such as ferrite magnets, per weight. In addition, the global supply of crucial rare-earth elements is uncertain, causing a real threat to the magnetic industry. Effective use of exchange coupling between hard and soft magnetic materials could decrease reliance on rare-earth based magnetic materials and lower the cost of high performance permanent magnets. Despite the promise, engineering a composite permanent magnetic material with enhanced magnetic properties as a result of exchange coupling has been an elusive goal. Research described in this thesis centers on the synthesis and characterization of metal-oxide 3D bulk composite materials for permanent magnetic applications. Samples were densified from powders using the Current Activated Pressure Assisted Densification (CAPAD) apparatus. A range of

samples with densities as high as 97% relative density have been synthesized in relatively short times (~10 minutes). Samples have been shown through X-ray diffraction (XRD) to contain desired composition, and are indeed hard and soft magnetic composites. The applied pressure has been shown to play a significant role in increasing density and in turn improving the magnetic properties. Enhanced magnetic saturation of the composite material, as compared to the mass dominant hard phase has been observed.

Table of Contents

List of Figures

Chapter 1: Introduction and Background

1.1 Motivation

Permanent magnetic materials are used extensively in the engineering industry. Digital memory, motors, generators, etc all rely on powerful magnets. The industry standards, Neodymium Iron Boride (Neo) or Samarium Cobalt magnets depend heavily on the use of rare earth elements. China, which produces 97% of the world's supply of rare-earth elements, has cut down exports of these valuable materials. As the world demand for rare-earth elements tripled from 2000 to 2010, China has cut exports from 48,500 tons to 31,310 tons [1]. Due to the increase in demand, decrease in supply, as well as other factors such as difficulty in processing and low corrosion resistance, Neo magnets cost 10 to 20 times more than Ferrite magnets, per pound [2]. A low cost replacement for rare-earth based magnets is vital for future permanent magnetic applications.

1.2 Basics of Magnetism

Magnetism, the response of a material to a magnetic field, has its roots in the sub-atomic level. Electron spins are the root cause of a magnetic response. The addition of all electron spin vectors gives rise to the net atomic magnetic moment μ_m. When an external magnetic field is applied, the potential energy of the system becomes

$$U = - \mu_m H \cos \theta \text{ [3]} \qquad (1)$$

where θ is 0^o in order to minimize potential energy, which is normally, the preferred energy state. This means that under an applied external magnetic field, magnetic moments will tend to orient themselves in the direction of the external field. Under a strong enough field, all of the magnetic moments will align in the direction of the external applied field and the sample is said to be saturated to saturation magnetization (M_s). Due to the magnetic moments of neighboring atoms (exchange energy), as well as extra activation energy usually needed to change moment direction (anisotropy energy), most saturated magnetic materials will keep some magnetization, even when an external applied magnetic field is removed. Neighboring magnetic moments will want to orient themselves in the same direction, for potential energy lowering purposes. The material property remanence (M_r) describes the amount of magnetization remaining, after an external applied magnetic field is removed from a saturated sample.

Some materials can be subject to a magnetic field and keep their initial magnetic orientation. This may seem strange since we've discussed that it is energetically preferential to orient magnetic movements in the direction of the applied field, however, many materials have easy and hard magnetization directions. Let us say we have a material with easy <100> family of directions and a hard <110> family of directions. If we saturate the material in the [100] direction and apply an external field in the [010] direction, the magnetic moment will have to pass the [110] hard direction, which increases magnetic anisotropy energy, and is energetically unfavorable. When the magnitude of potential energy due to an external field (Zeeman Energy) surpasses magnetic anisotropy energy and magnetic exchange energy, the moments will flip in the

direction of the external applied magnetic field. This gives rise to a material property called coercivity (H_c), which is the strength of an external applied magnetic field required to reduce the magnetization of a saturated sample to zero.

Numerous magnetic properties, especially those for permanent magnetic applications can be found by measuring magnetization as a function of applied magnetic field and plotting the data in a so called hysteresis loop. A hysteresis loop is shown schematically in **Figure 1.2.1**. A demagnetized sample is first saturated in one direction, then the opposite direction, and finally back to the original direction, forming a loop of magnetization versus external applied magnetic field. There are several scientific instruments capable of producing hysteresis loop measurement, including the Vibrating Sample Magnetometer (VSM) and the Superconducting Quantum Interference Device (SQUID).

A way to characterize the overall performance of a magnet as a permanent magnet is to look at a property called the energy product or BH_{max}. The BH_{max} is found by taking the largest rectangular area under the BH hysteresis loop in the second quadrant. The energy product and other magnetic properties are shown schematically in **Figure 1.2.1**. It is obvious that in order to attain a high energy product, both high remanence as well as high coercivity are needed.

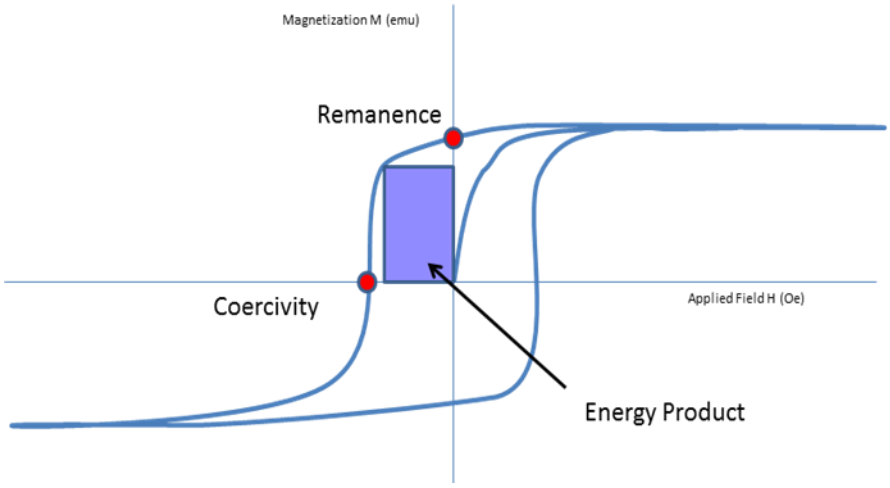

Figure 1.2.1: Schematic of a hysteresis curve showing various magnetic properties

1.3 Coercivity Dependence on Particle Size

Because coercivity is largely the resistance to the reversal of magnetic moments within the material, the magnetic structure within the material must be examined to gain better understanding. Permanent magnetic materials are generally made up of numerous magnetic domains. A magnetic domain is a region where all magnetic moments point in the same direction. When the net magnetic moment due to all of the domains inside the material is non-zero, the material acts as a permanent magnet and creates an external magnetic field. The formation of multiple domains inside a magnetic material is for potential energy lowering purposes. If a piece of magnet was a single domain, it would have a very large external magnetic field pointing away from the north pole and toward the south pole. The spacial extent of this external field could be decreased by dividing the material in smaller domains where the magnetic field travels from the north pole of one domain to the south pole of another. The subdivision onto multiple domains allows the magnetic material to decrease its magneto-static energy. However, it requires energy to keep a domain wall, because exchange energy is lowered when nearby moments point in the same direction. The size of domains in a material is largely a balance between magneto-static and domain wall energies:

$$Energy = Magnetostatic\ Energy + Domain\ Wall\ Energy \quad (2)$$

Grain size of a material has an incredibly large effect on the coercivity of the sample. Domain wall motion is largely the mechanism behind the demagnetization of a sample. If the grain size is very large, several domains may reside within one grain (magneto-static energy > domain wall energy). When an external magnetic field is

applied, the domains will merge into one, where all of the moments are oriented in the direction of the external applied magnetic field. The demagnetization process will be the reversal of rows of magnetic moments instead of all the moments all at once, since the grain is big enough to hold several domains. However, if the grain size matches the single domain size, then there can no longer be more than one domain per grain (domain wall energy > magneto-static energy). With a small grain, the demagnetization behavior can no longer be domain wall motion, since another domain can no longer nucleate. Instead, all of the magnetic moments within the grain must flip at the same time. Since it requires a higher field to flip all of the domains within a grain at once, than moving a domain wall, materials with grain sizes that match single domain size have increased coercivity. However, if the grain size is much smaller than the single domain size, thermal randomizing effects decrease coercivity, since there are fewer moments influencing each other to stay aligned, as shown schematically in **Figure 1.3.1**.

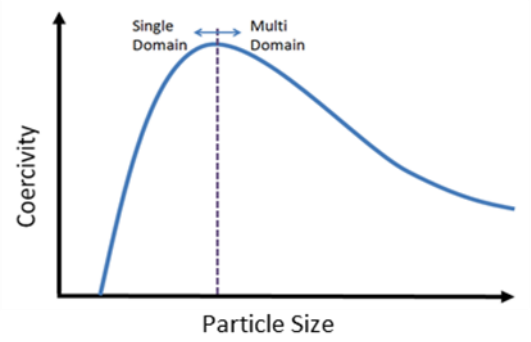

Figure 1.3.1 Schematic of the effect of grain size on coercivity [15]

1.4 Nano Composite Hard - Soft Exchange Coupled Magnet

Nano-scale materials have been of great interest in recent years because of their unique properties. The difference between nano-grain materials versus traditional ones is an increase in interface effects. Such effects are extremely beneficial in permanent magnetic applications through an exchange-coupled magnet. The proper combination of different magnetic materials could yield a more favorable magnetic response, than either of the two components [4].

The idea behind an exchange coupled magnet is well mixed phases of soft and hard magnetic materials sharing interfaces together. Individually, a hard magnet has high coercivity, but low saturation magnetization; while a soft magnet has very high saturation magnetization, but very low coercivity and remanence. Combining soft and hard magnetic materials in a composite magnet could take advantage of the high coercivity of the hard phase and the high saturation magnetization of the soft phase. A schematic of an exchange coupled material's hysteresis loop is shown in **Figure 1.4.1**. The soft material typically provides a much higher magnetic response than a hard material, but the problem is keeping the soft material's magnetic moments from flipping under and external applied magnetic field. At the interface between hard and soft grains, the moments of the soft material are affected by the magnetic field of the hard material and the soft material tends to stay aligned in the same direction as the hard material, minimizing potential energy, even under an applied external magnetic field. The exchange coupling phenomenon occurs, like most things, thanks to an overall lower potential energy of the system. Equation (1) describes potential energy due to exchange energy. It is clear that when

moment of nearby atoms point in the same direction (θ=0), exchange energy is minimized. The interaction between grains of soft and hard materials at the interface is the key to a successful exchange coupled magnet. Such interactions may be increased by maximizing the surface area of hard-soft interfaces. Relative surface area for nano-scale grains is much higher than that of traditional grain size magnets; exchange coupling could be taken advantage of in nano-composite materials.

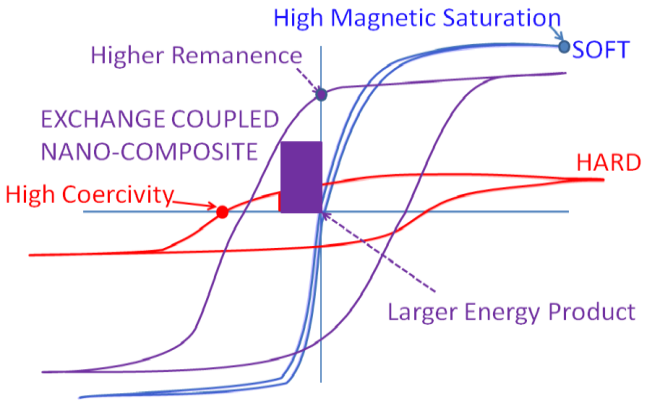

Figure 1.4.1 Schematic of an exchange coupled nano - composite hysteresis curve showing a much larger energy product and remanence of the composite, than either of the components

There has been much theoretical and experimental research done in the area of exchange coupled permanent magnets. A study by Fischer, Kronmuller from Germany and Fidler and Schrefl from Austria modeled grain size dependence on magnetic properties of nanocrystalline composite permanent magnets [5]. The study suggests that the highest energy product will be produced by increasing remanence, but keeping coercivity sufficiently high. M_r/M_s ratio of above 0.5 could be produced thanks to inter-grain exchange interactions. In another modeling study by the same group [6], the grain shape as well as soft phase grain size were discussed as they pertain to magnetic

behavior. It is predicted by model that small, regular shaped grains will have a minimal effect on decreasing coercivity in a nano-composite magnet. Their modeling study is supported by experimental evidence by M. Wilcox's group [7] where 10nm αFe particles in a Neo magnet matrix yield only slight decrease in coercivity. Sun's group from China put theory to practice and experimentally showed the benefits of a smaller soft phase grain size [8]. The exchange length,

$$Lex = \pi\sqrt{\frac{A}{K}} \quad [8] \qquad (3)$$

where A is the exchange energy constant and K is anisotropy energy constant, is the range of exchange interaction. The exchange length is effectively the domain wall width of the hard phase. Exchange energy, which is the energy that arises from nearby moment pointing in different directions, is minimized with wider domain wall width, since there is less of a rotation angle between adjacent moments. The anisotropy energy, which is the energy due to moments pointing in hard crystalline direction, is minimized in a small domain wall width, since there are fewer moments to point in unwanted hard directions. Equilibrium between the two energies dictated the domain wall width. Sun's group has calculated the exchange length of 7.5 nm for Neo-αFe composite magnet. They were able to show better coercivity and remanence in mechanically alloyed samples with soft phase grain size of 15nm vs. 27nm. In a more recent study, a collaborating group of Hao Zeng, Jing Li, J. P. Liu, Zhong L. Wang and Shouheng Sun from IBM, Louisiana Tech. and Georgia Tech. was able to successfully show exchange coupling of a FePt (hard)–Fe3Pt (soft) material system [9]. **Figure 1.4.2** clearly shows a coupled hysteresis curve as well as a hysteresis curve showing two phase behavior, reported by Zeng's group.

Microstructure effect on properties is clearly seen in both theoretical and experimental studies. It is clear that exchange coupled nano-composites are the way to the future of high performance magnets, however, no group listed was able to show exchange coupling in bulk. The studies reviewed were of annealed and/or mechanically alloyed powders, unusable in commercial applications.

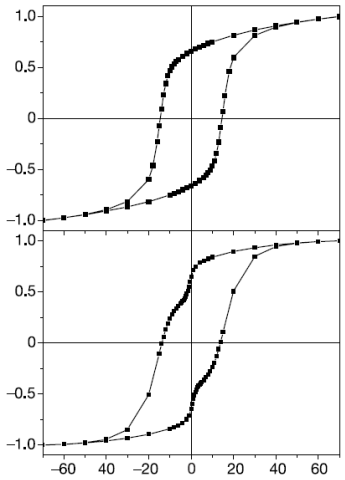

Figure 1.4.2 Hysteresis loops of coupled and uncoupled composite materials, showing coupled behavior in the top curve and two phase behavior in the bottom curve [9]

In this study, the focus will be on bulk 3D composite magnets of soft and hard magnetic phases. One hard magnetic phase and two soft magnetic phases were chosen for this study. The chosen hard magnetic material is Strontium Ferrite ($SrFe_{12}O_{19}$), henceforth referred to as SFO. The soft magnetic materials are Gamma Iron Oxide (γFe_2O_3) and Alpha Iron (αFe).

Strontium Ferrite was chosen as a base for the magnetic composite study. Hexa-ferrites, including Barium Ferrite and Lead Ferrite, are relatively inexpensive, and have one of the highest coercivities in the non rare-earth based magnet group. The fact that

Hexa-ferrites are oxides is an added bonus, since then can be exposed to atmosphere with no negative effects. Out of the three M-type ferrites (M for Ba, Sr or Pb), Strontium Ferrite was chosen because it is lead free, has the highest magnetic saturation [10], and some was readily available in the laboratory.

The structure of these M-type ferrites is called magnetoplumbite, see **Figure 1.4.3**. It is a hexagonal structure with a major preferred c axis and minor magnetically hard a axis. Oxygen atoms are close packed in the structure. Since Strontium, Barium and Lead ions are close in atomic radii to the Oxygen ions, they replace Oxygen in the lattice. Every fifth layer of the magnetoplumbite structure has an M-type ion substitution into an Oxygen site. Iron ions are found in interstitial sites of the structure. There are octahedral, tetrahedral and trigonal bi-pyramidal locations for Iron ions. The Fe^{3+} ions contribute a net moment of 4 Fe^{3+} ions in the up direction, yielding 20 μ_b per formula unit [11].

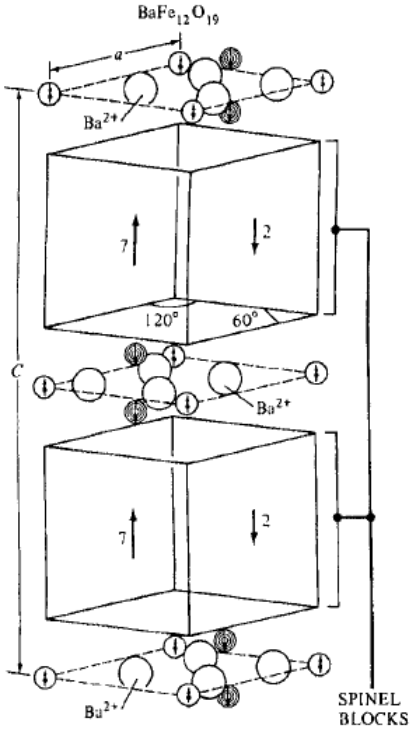

Figure 1.4.3 Magnetoplumbite structure of Barium Hexa-ferrite [11]

Thanks to SFO's easy c direction of magnetization, it is excellent to use as a permanent magnet. Magnetic moments have to go through the hard a direction of magnetization in order to flip under an applied field, contributing to SFO's high coercivity of 1500 - 3000 Oe [12].

Iron-Oxide (soft phase), one of the most abundant elements on earth, can be obtained at low cost. It is an excellent material to exchange couple with SFO and begin the composite magnet study. γFe_2O_3 has a theoretical saturation magnetization of 87.7 emu/g, which is higher than SFO's theoretical saturation magnetization of 75.6 emu/g [13]. Another exchange coupled system investigated is SFO and αFe (soft phase). αFe is

readily available and can be purchased safely in a micron particle size. αFe contributes a very high magnetic saturation at 245 emu/g [14]. Unlike the research done previously, this study will focus on bulk samples, that could be readily incorporated in real world applications.

1.5 Introduction to Densification

Thousands of years ago, humans made bricks by heating them up in ordered to promote strength. Ancient brick structures could still been seen all over the world. Heating clay brick to enhance properties is an early example of sintering. Today the sintering industry includes powder metallurgy, polymers, ceramics and cemented carbides [16].

Sintering involves consolidating fine particles into a bulk sample. Simply, the driving force for consolidation is the reduction of the surface free energy due to the decrease in total surface area by the reduction of solid-vapor boundaries. Solid-solid interfaces have a major reduction in curvature and hence surface energy, in comparison to their solid-vapor counterparts. Since the curvature of the fine particles plays a direct role in the sintering driving force, particles one the nanometer or micron scale are best suited for consolidation [17].

There are several mass transfer mechanisms in which small particles come together under elevated temperatures. First, sintering pressure arises when particles come together in order to decrease their surface area. A necking area forms between particles due to surface mass transfer. Particles undergo evaporation - condensation and surface

diffusion which does not cause densification, since the particle centers do not come together. Instead the low temperature mass transfer mechanics cause particle coarsening, or Ostwald Ripening [18]. At elevated temperatures, volume diffusion becomes the primary mass transfer mechanism, and densification occurs. It is imperative to reach higher temperatures quickly in order to retain small particle size by avoiding particle coarsening, and promoting densification.

Several variations sintering processes have been developed thought the history of the sintering industry. One process called pressure-less sintering involves powder placed in a mould, and heated to high temperatures in order to achieve high density. It is often difficult to achieve high densities with traditional sintering because of locked in porosity. As particles come together and consolidation occurs, pores could move from the inter-particle boundary and become trapped within the grain. Pressure could be introduced in order to help the densification process. A process called hot isostatic pressing (HIP) involves sintering in a pressurized gas environment. Pressure helps rearrange particles to a more favorable densification position, aid mass transfer and cause plastic deformation (especially in metals), in order to help achieve higher densities. Liquid phase sintering involves adding small amounts of powder that melts bellow densification temperature. The melt enters pores and helps remove locked in porosity, increasing the density of the final product. The hot pressing (HP) technique adds the benefits of directed pressure as well as high temperature in order to achieve samples with high densities; however the process could take hours due to slow heating rates [19].

1.6 Background of the CAPAD Process

Current Activated Pressure Assisted Densification (CAPAD) delivers very fast heating rates via joule heating, by running current directly through and/or around the powder being processed. Pressure is simultaneously applied in order to create high density samples in a matter of minutes, with high heating rates, typically ~ 200^{o}C/min. Current is ran though a water cooled electrode to a graphite diffuser, then to a plunger and die assembly and back out though another graphite diffuser and electrode, as shown in **Figure 1.6.1**. Powder is loaded into a die between two plungers. The die and plungers are typically made of high quality graphite, due to its excellent electrical and thermal conductive properties. The powder is densified under pressure, typically 100 MPa to 560 MPa and high temperature, typically 300^{o}C to 1000^{o}C. The device used in this work sits in an Instron 5580 frame with a load cell capable of delivering 160 kN. As discussed, temperature arises from Joule heating. Two Xantrex XDC DC power supplies provide current up to 2400 Amperes [19].

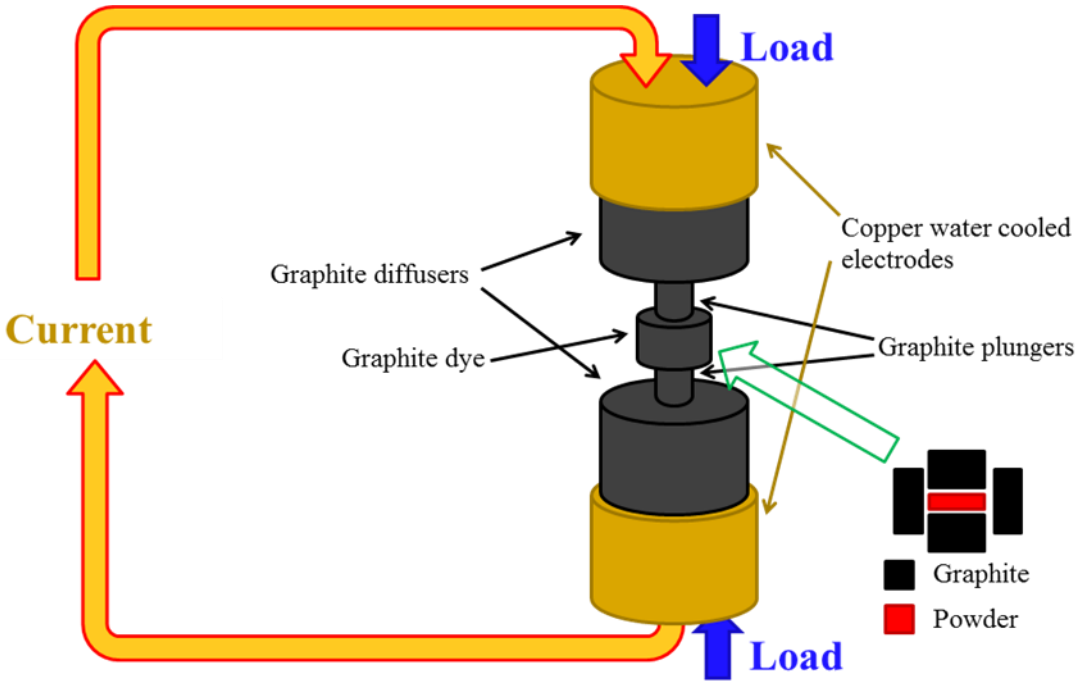

Figure 1.6.1 Schematic of a CAPAD set-up

1.7 Background of X-Ray Diffraction Characterization

Composition characterization could be acquired through X-Ray Diffraction. When X-Rays are shot at a crystalline material, due to light's waive-like behavior, interference with atoms is possible. When the X-Rays interfere constructively with the atoms of a crystalline material, the signals intensity on the receiving end is high. Because the material is crystalline, spacing between atomic planes is a function of atomic plane's miller indices (hkl) and the material lattice parameter a.

$$d = \frac{a}{\sqrt{h^2+k^2+l^2}} \qquad (4)$$

Since most crystalline materials have unique lattice parameters, by knowing the inter-planar distance and the miller indices, the lattice parameter could be determined. Bragg's Law shows the relationship between angles (measured from a horizontal) at which constructive interference occurs, inter-planar distance and wavelength.

$$n\lambda = 2d \sin\theta \qquad (5)$$

By comparing X-Ray diffraction pattern with known standards, material phases in a powder or bulk sample could be characterized.

Chapter 2: Procedure

2.1 Powder Processing

Starting powders were obtained from commercial sources. Strontium Hexa-Ferrite (SFO) was bought from NanoAmor. The powder is reported 99% pure with an average size of 800nm. γFe_2O_3 was bought from Advanced Materials. Nano size αFe was purchased from NanoAmor. Nano αFe (Nano-Fe) powder was reported 99.5% pure with a particulate size of 25nm. Micro size αFe was purchased from Sigma Aldrich. Micro αFe (Micro-Fe) powder was reported 99.9% pure, with an average particulate size of <10 microns.

2.1.1 Monolithic Sample Powder Preparation

For monolithic densified samples, powder preparation involved loading the as received powders into a graphite dye (for Nano-Fe, this was done in a glovebox), between two graphite plungers. Two thin sheets of graphite foil were placed on the top and bottom of the powder, so that if a bond to graphite was formed, the graphite sheets could be easily polished off, instead of having to cut the densified sample from the plungers. The plungers were hand pressed to keep the dye from sliding. The dye, plunger and powder assembly was transferred into the CAPAD device for processing.

2.1.2 Composite Sample Powder Preparation

When making composite densified samples, prior to consolidation, starting powders were measured out in desired mol ratios and mixed together. In order to achieve homogeneous mixing, the powders were first mixed together using a mortar and pestle. The mixed powders were placed in a jar with 3mm diameter zirconia balls and swirled around for of up to 24 hours at 20 - 80 rpm (low energy milling). Powder was scraped from the walls every 4 hours.

2.1.3 High Energy Planetary Ball Milling Powder Preparation

In order to tailor the microstructure of consolidated samples, great attention must be given to powder preparation. High energy planetary ball milling was used to tailor the average particulate size of the pre-consolidated powder. High energy milled composite sample powder preparation included mixing the starting powders with mortar and pestle, low energy tumble milling the mixed powders, as discussed in **Section 2.1.2** and loading the low energy milled powder into stainless steel jars with 3mm diameter stainless steel balls, at powder to ball weight ratio of 1 g powder to 10 g balls. The jar ball and powder assembly was then placed into a Fritsch Planetary Micro Mill Pulverisette 7 Premium Line planetary high energy ball mill. High energy milling parameters ranged in time of 3 hours to 72 hours at 300 rpm.

2.2 Densification in the CAPAD

A typical Current Activate Pressure Assisted Densification (CAPAD) run involves loading the processed powder into the plunger and die assembly as described in **Section 2.1**. If the powder is atmosphere sensitive, the loading is done within a glove box. The plunger and die assembly is then transferred into the CAPAD chamber, where it is placed between two graphite diffusers.

2.2.1 Graphite Plunger System

Powder inside the dye and plunger assembly is pre-pressed at 70MPa for 60 seconds in order to avoid any packing differences between runs. The chamber is placed under vacuum in order to have consistent and neutral atmosphere between runs. After a pressure of $5x10^{-2}$ Torr is reached, 2 volts are applied on the electrodes by the power supplies. A pressure ramp by the Instron load frame is simultaneously started at the rate of 5 kN/min; at the end of the pressure ramp, the typical load is 30 kN or 104 MPa of pressure. As soon as the maximum load is reached, voltage is ramped at the rate of 0.25 volts every 20 seconds, until desired temperature is attained. The sample could be held at temperature, in which case a PID controller adjusts the current to keep desired temperature, or the run could be ended by turning off the power supplies and relieving the load off the sample. **Figure 3.2.1** shows die temperature, power supply voltage, extension and load as a function of time in a typical 5 minute hold time CAPAD experiment. At the end of the process, cylindrical samples typically the size of a nickel coin, 19mm in diameter and about 1 mm in thickness, are extracted from the die and plunger assembly.

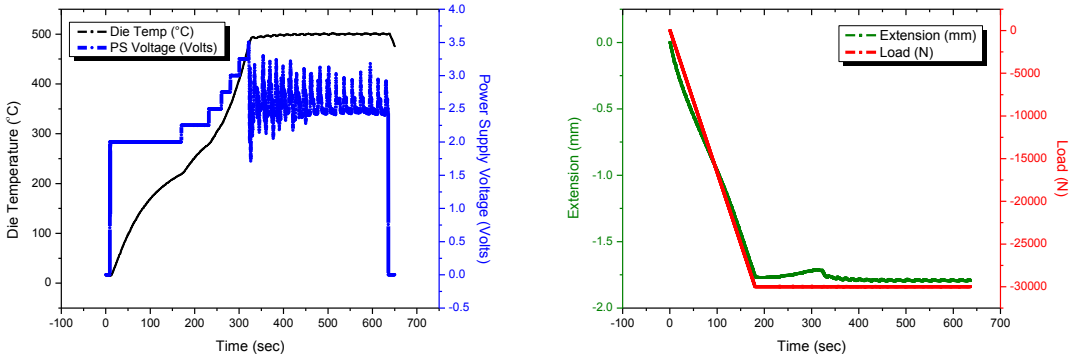

Figure 2.2.1 Typical CAPAD run with a 5 minute hold time

2.2.2 Tungsten Carbide (WC) Plunger High Pressure System

Under some circumstances, a high pressure system was used to achieve densification pressure of up to 250 MPa. This system involved switching traditional graphite plungers for tungsten carbide plungers, as shown schematically in **Figure 2.2.2.1**. WC plungers with exact diameter specifications were purchased from Sentential Carbide. The plungers were then ground to flat to provide perfect incorporation into the CAPAD system. Two stainless steel pucks where also machined to provide a pressure relief layer for the graphite diffusers.

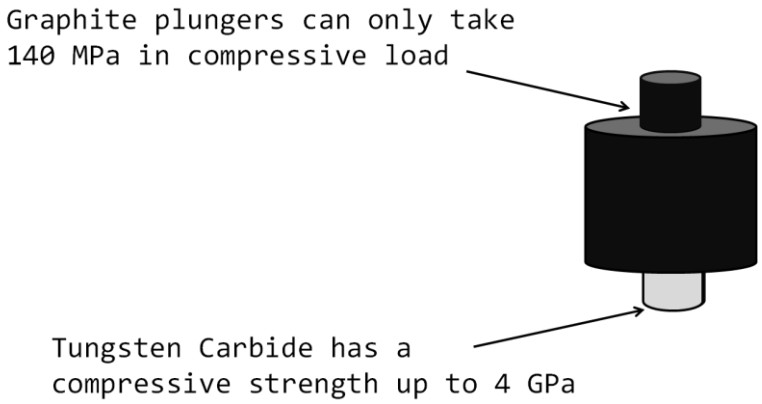

Figure 2.2.2.1 Schematic showing replacing graphite plungers with WC plungers [24]

Tungsten Carbide has a much higher compressive strength than graphite, allowing for higher densification pressures. The pressure limitation of this system lies in the stainless steel pucks placed on top and bottom of the plungers within the CAPAD to diffuse the pressure felt by the graphite diffusers. Creep failure is seen in stainless steel at pressures of 250MPa and temperatures of 550^{o}C. In some instances, higher densification pressure was required. In order to achieve even higher densification pressure, the area of the samples was reduced by using a smaller mini graphite dye and tungsten carbide plunger system within the larger graphite dye and tungsten carbide plunger system, shown schematically in **Figure 2.2.2.2**. Since the larger tungsten carbide plungers relieve the pressure felt by the stainless steel pucks, creep within the pucks is no longer an issue. Densification pressures of up to 560MPa are attainable using the mini tungsten carbide system.

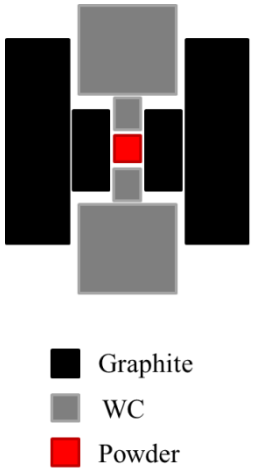

Figure 2.2.2.2 Schematic showing WC mini system set-up

2.3 Sample Characterization and Property Measurement

Several sample properties were measured after densification. Some properties that were measured include coercivity, remanence and energy product. Sample composition and density were also characterized.

2.3.1 Density Measurement

The density of a sample is a major indication of success of the densification process. Density was measured geometrically, by using known die diameter and averaging numerous sample thickness measurements taken with calipers. Archimedes density measurement was not used because numerous samples had low densities, and high porosity for water to seep into the sample. Wrapping samples with Parfilm for Archimedes density measurements gave unreliable results (poor precision), so geometrical density measurements were chosen for their high precision.

2.3.2 Composition Characterization

The composition of the samples was characterized using x-ray diffraction (XRD). Both densified samples and starting powders were characterized. XRD data was collected using a Bruker D8 Advance X-Ray Diffractometer. Intensity peaks were compared with Inorganic Crystal Structure Database (ICSD) [20]. Compositional data was deduced by comparing measured diffraction pattern with ICSD standards. If the sample showed evidence of peaks from two different compositions, the relative composition of each could be attained by looking at the difference in peak intensity.

2.3.3 Magnetic Measurements

Magnetic measurements of samples were done on both a Superconducting Quantum Interference Device (SQUID), and a Vibrating Sample Magnetometer (VSM). The SQUID device was Quantum Design's XL MPMS model, capable of applying fields up to 7 Tesla, while Lake Shore's VSM is only capable of applying fields of up to 1.7 Tesla. While the SQUID is a more sensitive and powerful instrument, it requires liquid helium cooling; its design incorporates superconducting regions. The SQUID is very expensive to operate. The VSM on the other hand uses water-cooled electro-magnets to create a magnetic field. A pickup coil measures sample magnetization by recording induced current. The VSM is a much cheaper and faster machine for generating hysteresis loops measurements.

Samples measured in both SQUID and VSM were cut down to rectangles with dimensions of about 3mm by 3mm by 1mm in order to produce a magnetic response in

the range of the pickup system. Samples were demagnetized prior to magnetic measurement. The VSM was calibrated with a standard piece of Nickel with a known magnetic response. The derived hysteresis loop was used to record coercivity and magnetic remanence. The energy product was calculated from data collected by the SQUID. VSM's internal software provided the energy product, and was checked for accuracy.

2.3.4 Microstructure Characterization

Electron microscopy was used to characterize sample microstructure. Electron micrographs have been generated for both densified samples and starting powders. A Philips XL-30 scanning electron microscope was used to produce the micrographs. Secondary electron (SE) micrographs, showing topography, were used to observe the shape, size and agglomeration of starting powders. SE micrographs of fracture surfaces gave an idea of the residual porosity as well as topography of densified samples. Back scattered electron (BSE) micrographs were used to confirm phase purity of starting powders as well as to observe the phase separation and degree of homogeneity of grains in a densified sample.

Chapter 3: Results

Densified samples' processing parameters are summarized in the **Table 3.1** for ease of reference. Sample name column gives name to a densified sample. Starting powder column presents the mol to mol ratio of pre-consolidated powders. Unless otherwise stated, starting powders were mixed using a mortar and pestle, as well as low energy tumble milling as described in **Section 2.1**. Densification pressure describes the maximum pressure the powder was exposed to during the CAPAD process. Densification temperature describes the maximum temperature the powder was exposed to during the CAPAD process. Hold time describes the length of time that starting powder was exposed to densification pressure and temperature during the CAPAD process. Relative density shows the relative density of the densified sample, as compared to the actual density of its phase(s):

Table 3.1 Densified Samples:

Sample Name	Starting Powder	Densification Pressure (MPa)	Densification Temperature (^{o}C)	Hold Time (seconds)	Relative Density (%)
SFO_1	NanoAmor SFO	104	1000	0	86
NanoFe_1	NanoAmor Fe	104	950	0	70
MicroFe_1	Sigma Aldrich Fe	104	900	0	96
SFO_Fe_2O_3_1	SFO:γFe_2O_3	104	1000	0	87
SFO_Fe_2O_3_2	SFO:$2\gamma Fe_2O_3$	104	1000	0	95

SFO_Fe_2O_3_3	SFO:3γFe_2O_3	104	1000	0	98
SFO_Fe_1	SFO:6Fe	104	500	0	65
SFO_Fe_2	SFO:6Fe	104	600	0	70
SFO_Fe_3	SFO:6Fe	104	700	0	88
SFO_Fe_4	SFO:6Fe	104	750	0	93
SFO_Fe_5	SFO:6Fe	140	500	0	66
SFO_Fe_6	SFO:6Fe	104	500	300	67
SFO_Fe_7	SFO:6Fe	104	550	0	71
SFO_Fe_8	SFO:12Fe	104	450	0	62
SFO_Fe_9	SFO:12Fe	104	500	0	64
SFO_Fe_10	SFO:12Fe	104	550	0	81
SFO_Fe_11	SFO:12Fe	104	600	0	87
SFO_Fe_12	SFO:3Fe	407	500	120	86
SFO_Fe_13	SFO:6Fe High Energy	407	500	120	97
SFO_Fe_14	SFO:12Fe	140	500	0	75
SFO_Fe_15	SFO:12Fe	104	500	0	64
SFO_Fe_16	SFO:12Fe	140	500	0	67
SFO_Fe_17	SFO:12Fe	104	500	0	63
SFO_Fe_18	SFO:3Fe	407	500	120	86
SFO_Fe_19	SFO:6Fe	300	500	60	74
SFO_Fe_20	SFO:3Fe High Energy	407	500	120	90

3.1 Characterization and Properties of Starting Powders and Monolithic Samples

Starting powder has great importance in the outcome of bulk densified samples. Shape, agglomeration, purity of powder could greatly affect the success of a material system study.

3.1.1 Stontium Hexa-ferrite (SFO)

SFO powder is reported 99% pure with an average size of 800nm. **Figure 3.1.1.1, Figure 3.1.1.2, Figure 3.1.1.3 and Figure 3.1.1.4** show SE micrographs of starting SFO powder. The powder has an observed particulate size of 300nm to 3µm. Some particulates are hexagonal in shape, and very thin. **Figure 3.1.1.4** show a BSE micrograph of starting SFO powder. The contrast within the particulates is uniform.

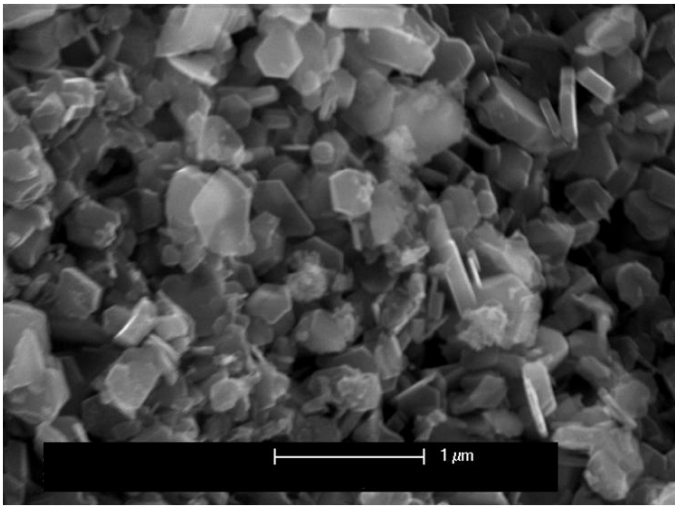

Figure 3.1.1.1 SEM micrograph of SFO starting powder (SE)

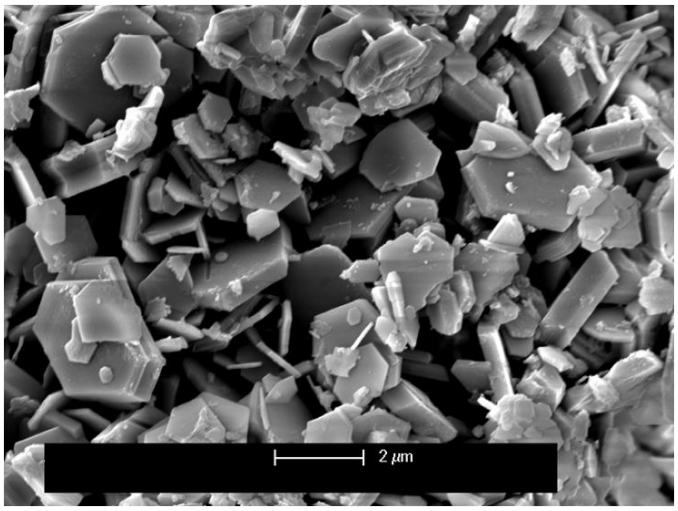

Figure 3.1.1.2 SEM micrograph of SFO starting powder (SE)

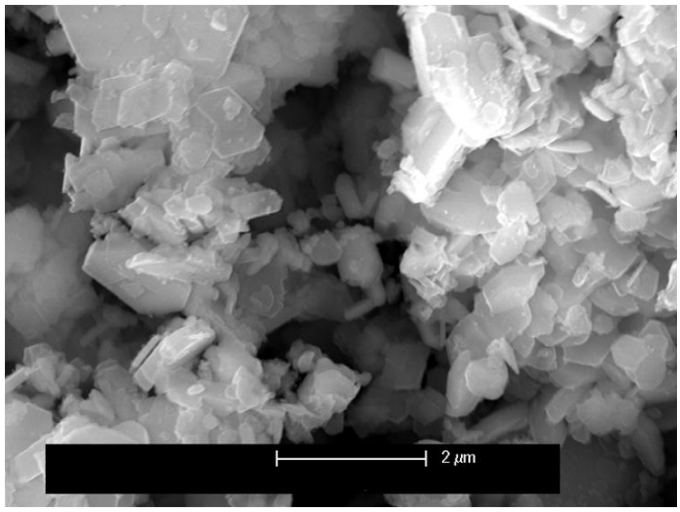

Figure 3.1.1.3 SEM micrograph of SFO starting powder (SE)

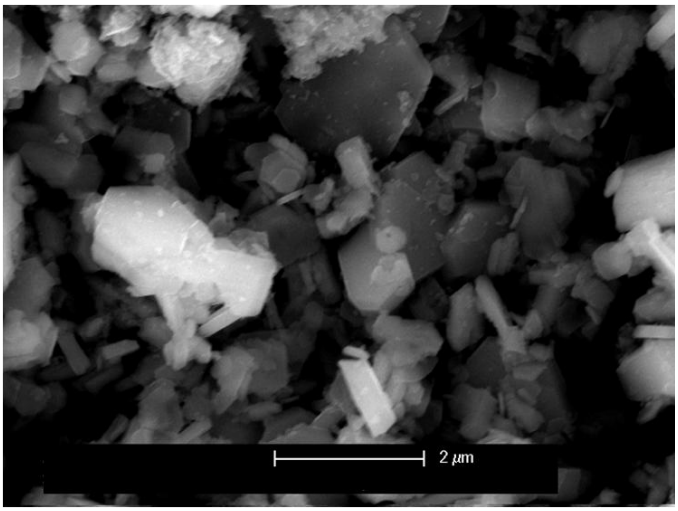

Figure 3.1.1.4 SEM micrograph of SFO starting powder (SE)

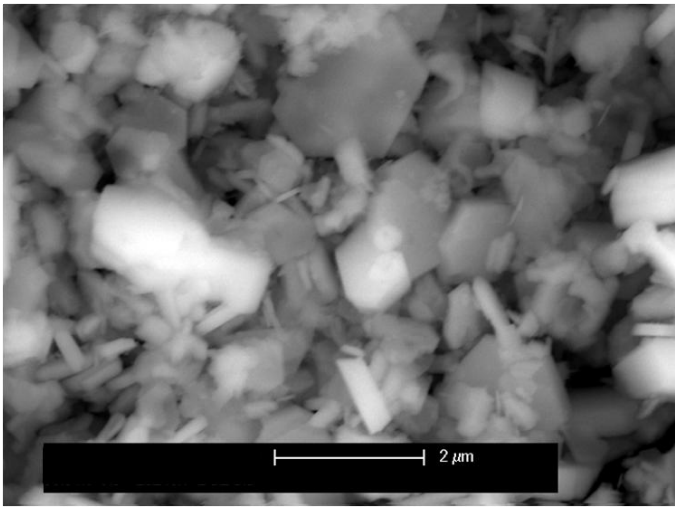

Figure 3.1.1.5 SEM micrograph of SFO starting powder (BSE)

Figure 3.1.1.6 displays an XRD profile of SFO as received powder in comparison to an ICSD SFO standard, confirming phase purity.

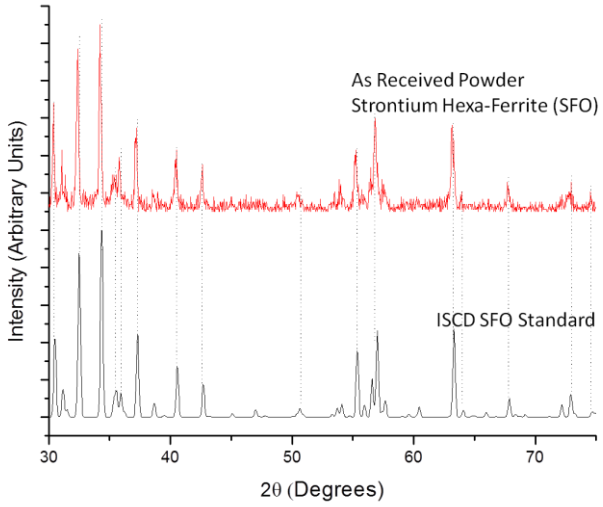

Figure 3.1.1.6 XRD profile of SFO
starting powder showing phase purity

Figure 3.1.1.7 shows the hysteresis curve of a densified SFO sample (SFO_1). The curve was measured at room temperature using the SQUID. Sample measured was densified at 104MPa and 1000^{o}C. The sample is 86% dense. As expected, high coercivity of 2400 Oe is observed in this material with high magnetic anisotropy.

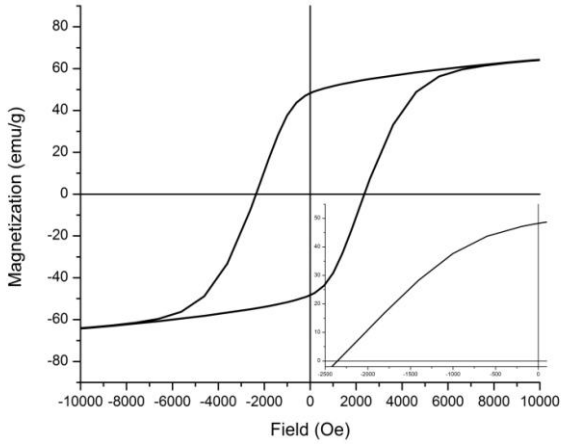

Figure 3.1.1.7 Hysteresis curve of densified SFO (SFO_1) showing a BHmax of 1.02 MGOe

3.1.2 Nano-Fe

Fe with an average reported particulate size of 25nm was commercially purchased. The powder is reported 99.5% pure. **Figure 3.1.2.1, Figure 3.1.2.2 and Figure 3.1.2.3** show SE micrographs of the starting powder with very small grains (>50nm) in very large agglomerations (>50μm). **Figure 3.1.2.4** shows a BSE micrograph with similar contrast within the Fe particulates.

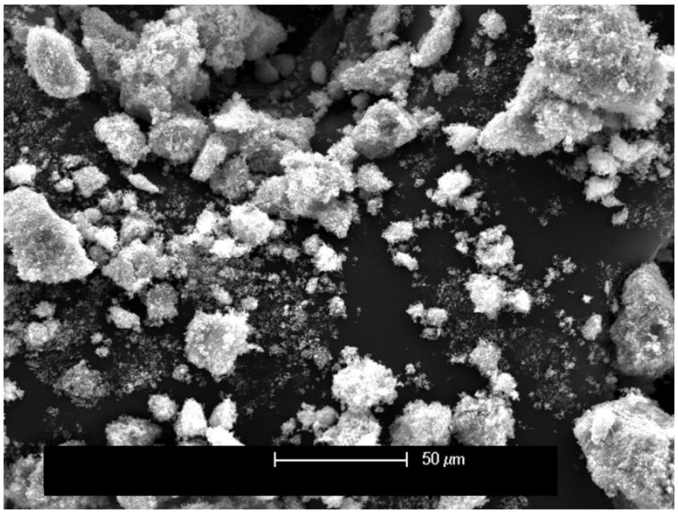

Figure 3.1.2.1 SEM micrograph of Nano-Fe starting powder (SE)

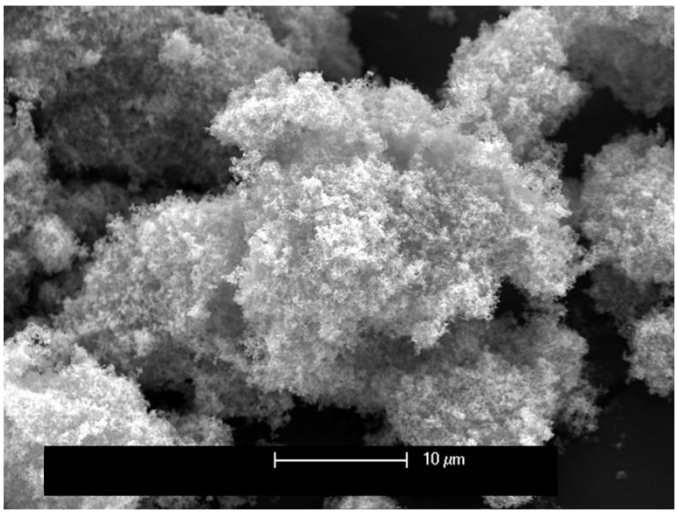

Figure 3.1.2.2 SEM micrograph of Nano-Fe starting powder (SE)

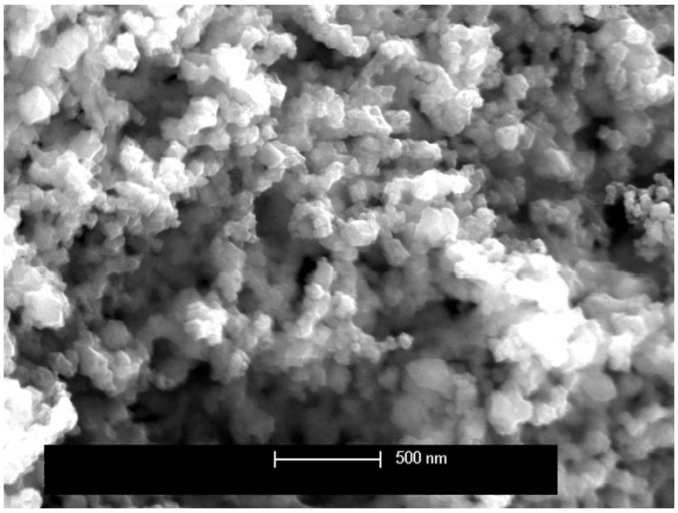

Figure 3.1.2.3 SEM micrograph of Nano-Fe starting powder (SE)

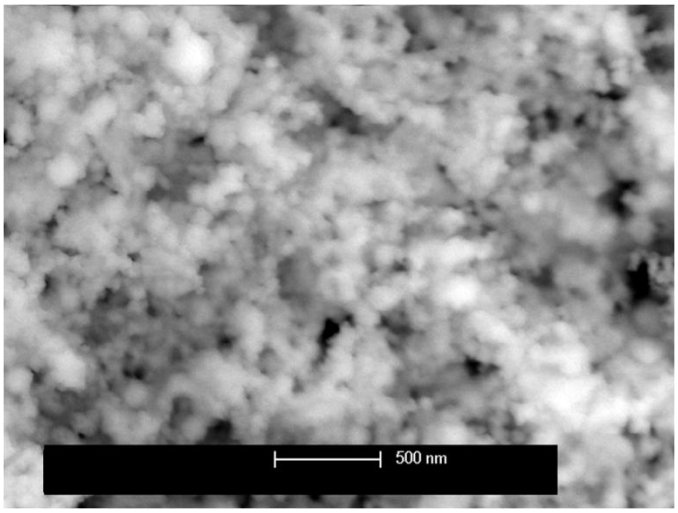

Figure 3.1.2.4 SEM micrograph of Nano-Fe starting powder (BSE)

Figure 3.1.2.5 displays an XRD profile of a monolithic densified sample of Nano-Fe (NanoFe_1) compared to ICSD standards of Fe and FeO. The densified sample (NanoFe_1) displays a high volume fraction of FeO as well as some Fe.

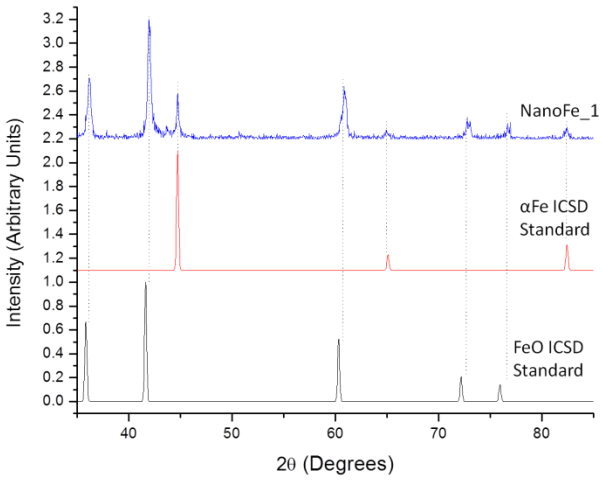

Figure 3.1.2.5 XRD profile of Nano-Fe densified sample (NanoFe_1) showing that the majority of composition is FeO

Figure 3.1.2.6 shows a hysteresis curve of CAPAD densified sample of Nano-Fe (NanoFe_1). The curve was measured at room temperature using the SQUID. Sample measured was densified at 104MPa and 950^{o}C. The sample is 70% dense, assuming pure Fe composition. At only 35 emu/g, the magnetic saturation of the densified sample is much less than expected.

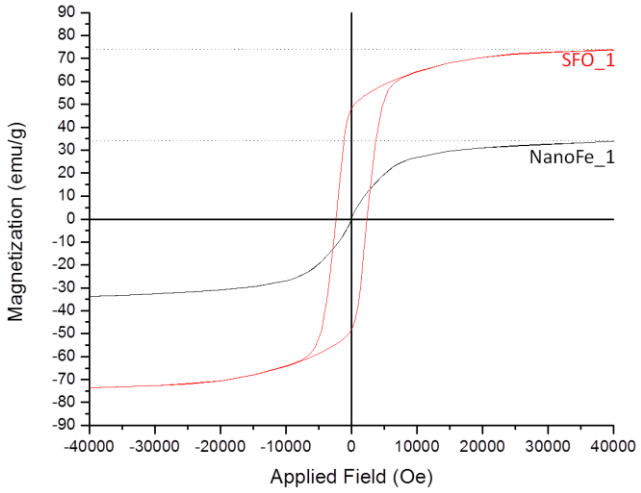

Figure 3.1.2.6 Hysteresis curve of densified Nano-Fe (NanoFe_1), showing a much lower saturation magnetization than densified SFO (SFO_1)

3.1.3 Micro-Fe

Fe powder with 99.9% purity was purchased commercially. The powder is claimed to have <10 μm crystallite size. **Figure 3.1.3.1, Figure 4.1.3.2, Figure 3.1.3.3 and Figure 3.1.3.4** show SE micrographs of micro-Fe starting powder, confirming the advertised crystallite size. **Figure 3.1.3.5** displays a BSE micrograph showing no contrast difference within the micro-Fe starting powder crystallites.

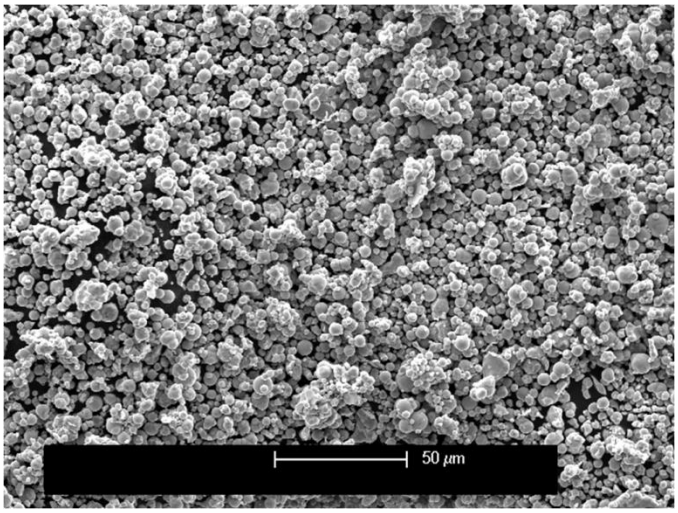

Figure 3.1.3.1 SEM micrograph of Micro-Fe starting powder (SE)

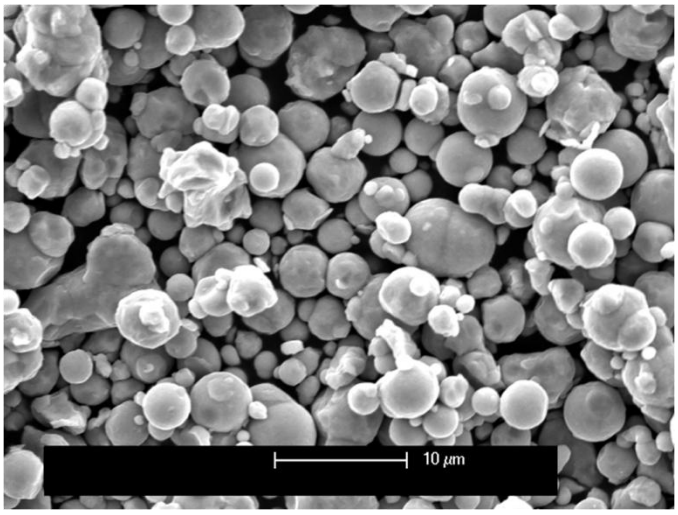

Figure 3.1.3.2 SEM micrograph of Micro-Fe starting powder (SE)

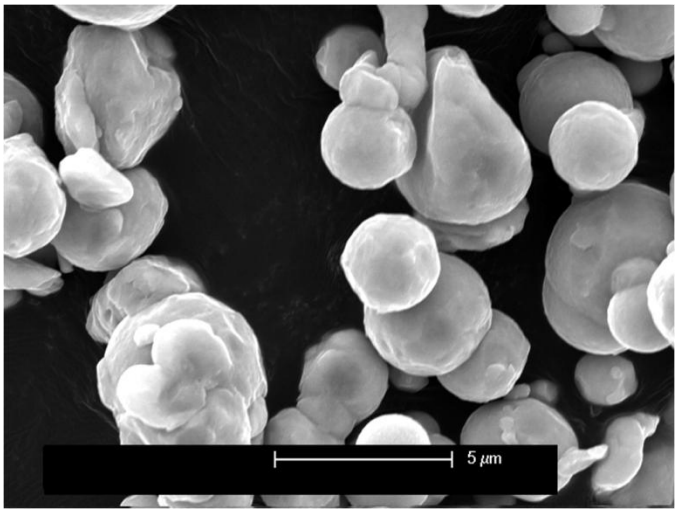

Figure 3.1.3.3 SEM micrograph of Micro-Fe starting powder (SE)

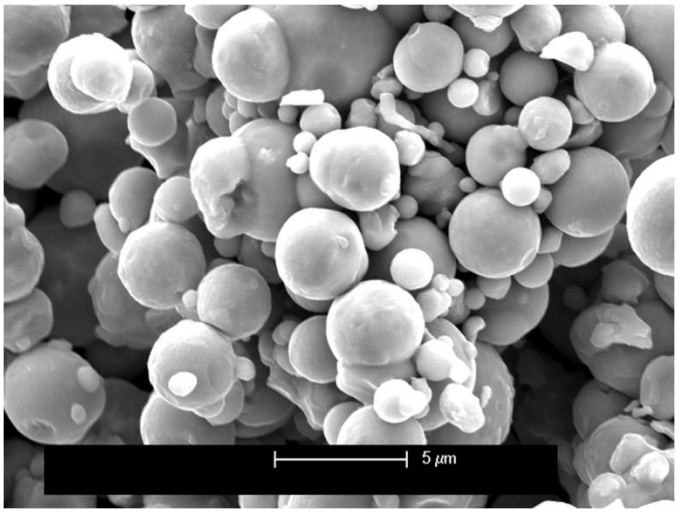

Figure 3.1.3.4 SEM micrograph of Micro-Fe starting powder (SE)

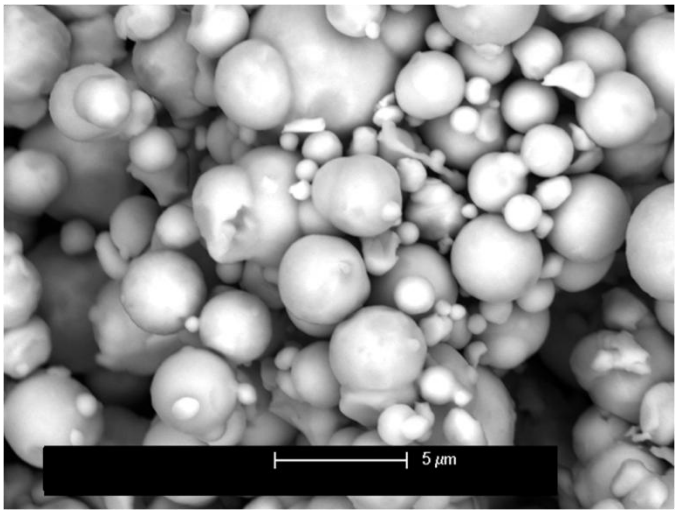

Figure 3.1.3.5 SEM micrograph of Micro-Fe starting powder (BSE)

Figure 3.1.3.6 shows an XRD profile of Micro-Fe as received powder as well as a CAPAD densified Micro-Fe sample. αFe phase purity is confirmed.

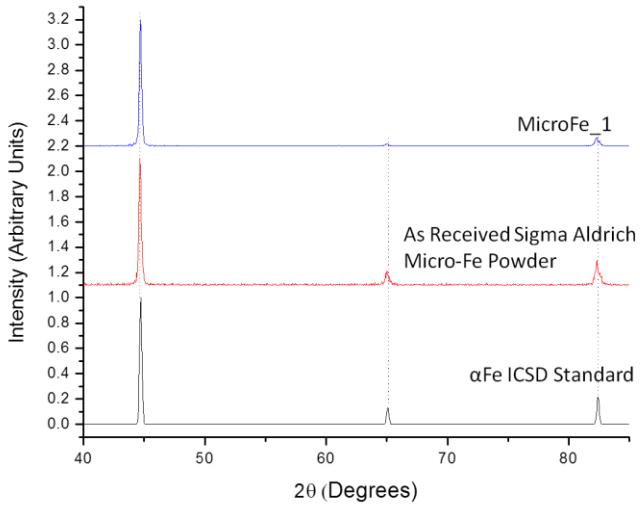

Figure 3.1.3.6 XRD Profile of Micro-Fe starting powder as well as a Micro-Fe densified sample (MicroFe_1) showing phase purity in both densified sample and starting powder

Figure 3.1.3.6 displays a hysteresis curve of Micro-Fe densified sample (MicroFe_1), measured at room temperature using the VSM. Sample measured was densified at 104MPa and 900^{o}C. The sample is 96% dense. Very high saturation magnetization of 240 emu/g is observed. Micro-Fe has a much higher saturation magnetization than SFO.

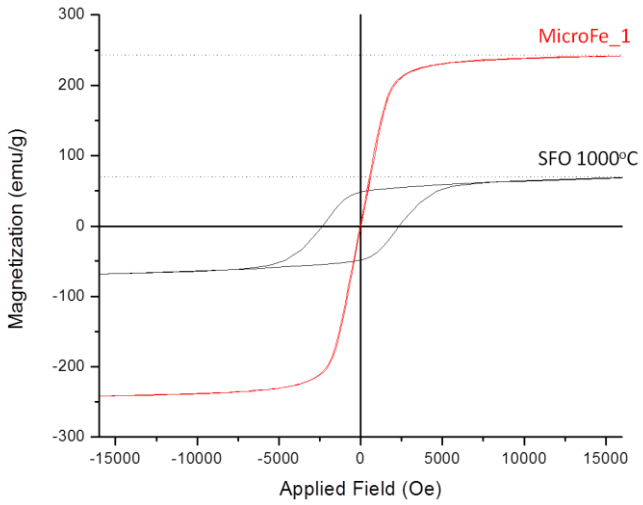

Figure 3.1.3.6 Hysteresis curve of densified Micro-Fe (MicroFe_1), showing a much higher saturation magnetization than densified SFO (SFO_1)

3.2 SFO - Fe-O

A study of the SFO - γFe_2O_3 material system was performed. Magnetic properties of the 1:1 (SFO_Fe_2O_3_1), 1:2 (SFO_Fe_2O_3_2) and 1:3 (SFO_Fe_2O_3_1) mol SFO to mol γFe_2O_3 compositions were measured at room temperature and the hysteresis loop reported in **Figure 3.2.1**.

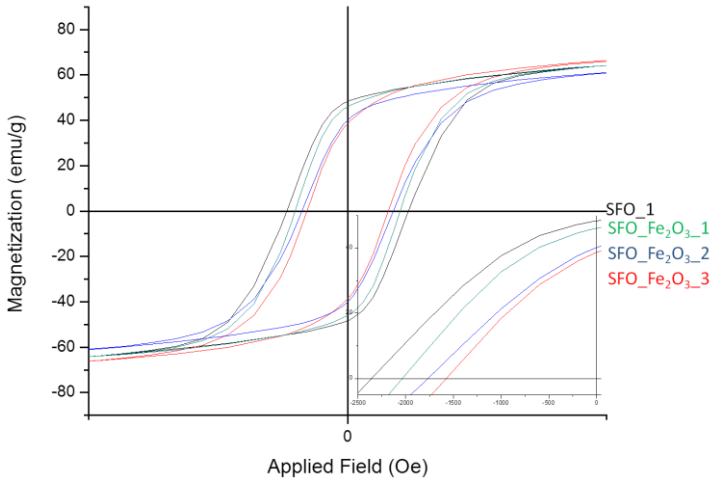

Figure 3.2.1 Hysteresis curves of densified SFO - γFe_2O_3 samples, showing a composition sweep; lower magnetic properties, than those of densified SFO sample (SFO_1), are observed

3.3 SFO - Micro Fe

SFO was mixed with Micro-Fe powder. The powders were prepared using the procedure detailed in **Section 2.1**. Three mixtures of 1 mol SFO to 3 mol Fe (SFO - 3Fe), 1 mol SFO to 6 mol Fe (SFO - 6Fe), and 1 mol SFO to 12 mol Fe (SFO - 12Fe) were produced.

3.3.1 SFO - 6Fe Processing Temperature Study

Figure 3.3.1.1 displays XRD profiles of SFO - 6Fe densified samples. Desired composition is observed at 500°C. At 600°C and above, XRD profile peaks of FeO are observed.

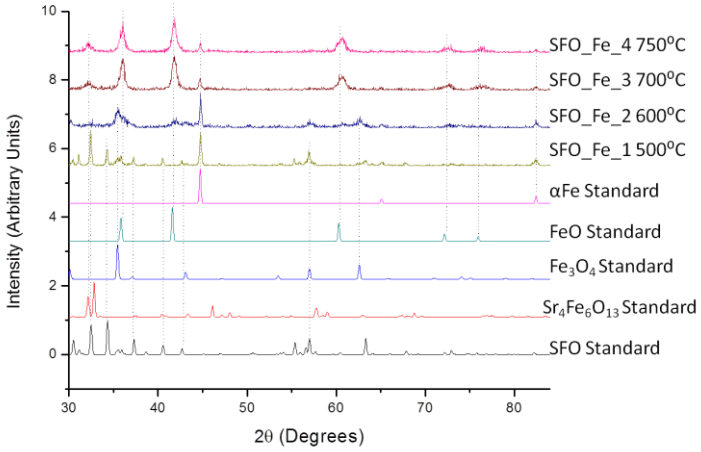

Figure 3.3.1.1 XRD Profile showing a temperature study of SFO - 6Fe densified composite samples, displaying reaction at temperatures above 500°C

3.3.2 SFO - 6Fe CAPAD Parameter Modifications

Figure 3.3.2.1 displays an XRD profile, showing the effects of slight increase in temperature, pressure and hold time on the SFO - 6Fe composite material system. Desired composition is observed under each densification parameter modification.

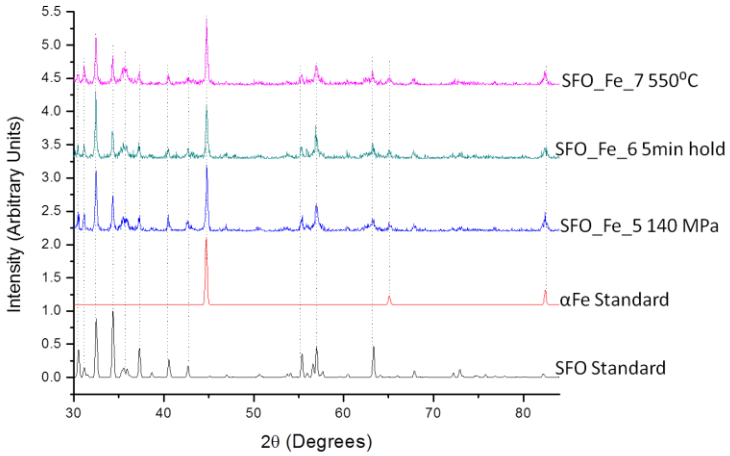

Figure 3.3.2.1 XRD profile of densified SFO - 6Fe composite samples showing CAPAD parameter modifications in temperature, pressure and hold time, displaying SFO and Fe phases still present within the composite

3.3.3 SFO - 12Fe Processing Temperature Study

Figure 3.3.3.1 displays an XRD profile of densified SFO - 12Fe composite samples. A temperature sweep using densified samples was studied to determine the effect of higher densification temperature on the composition of composite samples with a high Fe content. FeO's x-ray diffraction peaks are observed at temperatures of 500°C and above.

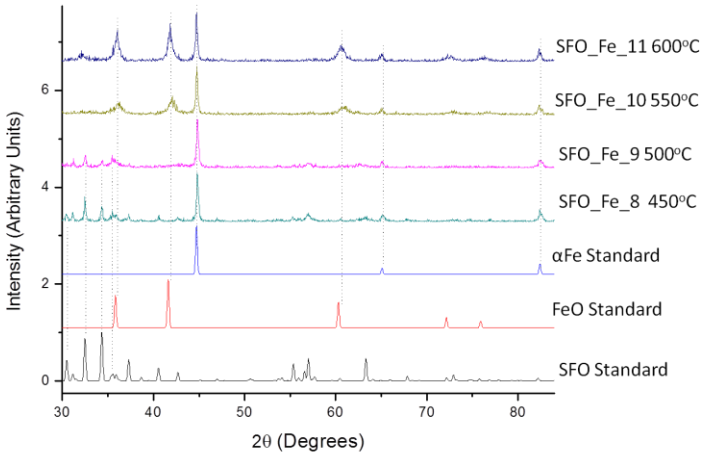

Figure 3.3.3.1 XRD profile of densified SFO - 12Fe composite samples showing a temperature study, displaying reaction in densified samples at temperatures above 500°C

3.3.4 SFO - 3Fe Microstructure Analysis

Figure 3.3.4.1, Figure 3.3.4.2 and Figure 3.3.4.5 show SE micrographs of a densified SFO - 3Fe composite sample (SFO_Fe_12). Samples densified from 1 mol SFO to 3 mol Fe powder where polished using silicon carbide paper. SE micrographs show different topography of Fe and SFO grains, as well as numerous pores. **Figure 3.3.4.2 and Figure 3.3.4.6** display BSE micrographs of densified SFO - 3Fe composite. Iron, SFO and porosity phases can be clearly identified. Fe grains appear to have much lighter contrast than SFO since the effective atomic number of Fe, Z_{Fe},is larger than Z_{SFO}.

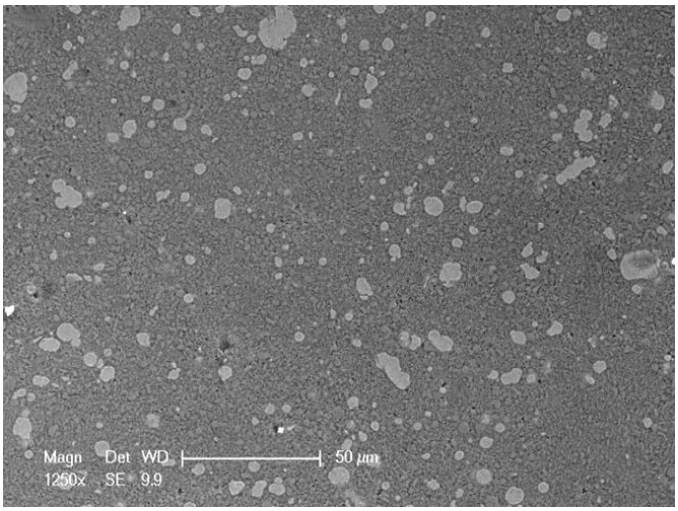

Figure 3.3.4.1 SEM micrograph of densified SFO - 3Fe composite sample (SFO_Fe_12) showing large Fe grains (SE)

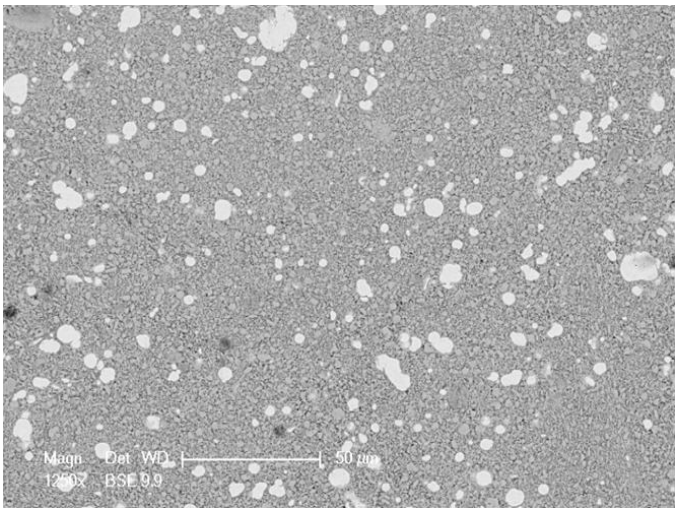

Figure 3.3.4.2 SEM micrograph of densified SFO - 3Fe composite sample (SFO_Fe_12) showing large Fe grains (BSE)

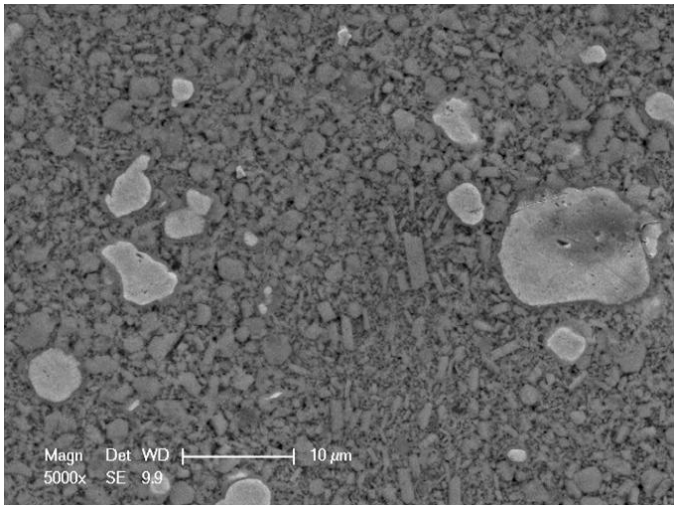

Figure 3.3.4.3 SEM micrograph of densified SFO - 3Fe composite sample (SFO_Fe_12) showing large Fe grains (SE)

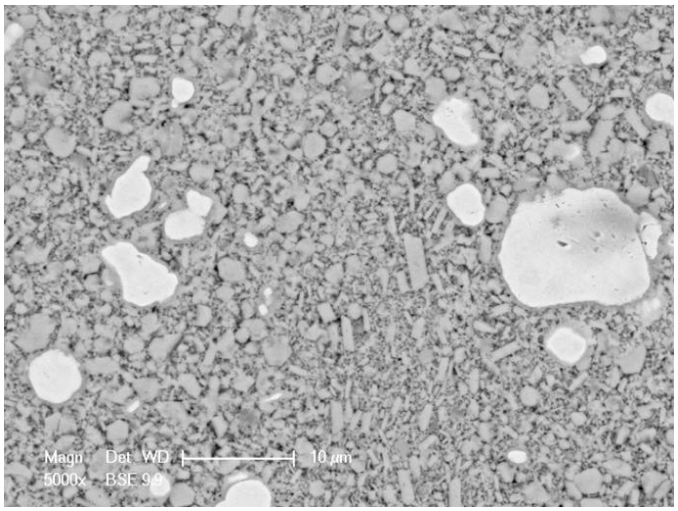

Figure 3.3.4.4 SEM micrograph of densified SFO - 3Fe composite sample (SFO_Fe_12) showing large Fe grains (BSE)

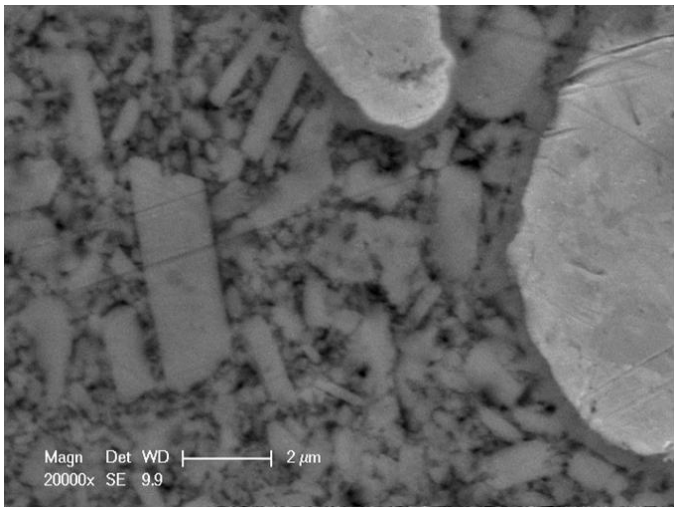

Figure 3.3.4.5 SEM micrograph of densified SFO - 3Fe composite sample (SFO_Fe_12) showing a clear SFO/Fe boundary (SE)

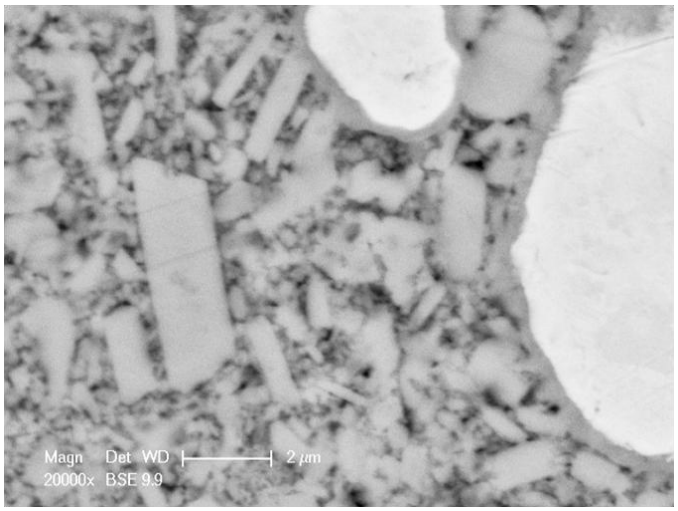

Figure 3.3.4.6 SEM micrograph of densified SFO - 3Fe composite sample (SFO_Fe_12) showing a clear SFO/Fe boundary (BSE)

3.3.5 SFO - 6Fe High Energy Planetary Ball Milling

Figure 3.3.5.1 displays an XRD profile of densified SFO - 6Fe composite sample made from low energy milled powder (SFO_Fe_19), starting SFO - 6Fe powder after high energy planetary ball milling (SFO:6Fe high energy powder), and densified SFO - 6Fe composite sample made from high energy milled powder (SFO_Fe_13). While desired composition is observed in the densified composite sample made from low energy powder, as well as pre-densified high energy powder; densified composite sample made from high energy powder shows evidence of reaction. Both the low energy and high energy milled densified samples were densified at 500^{o}C and 104MPa.

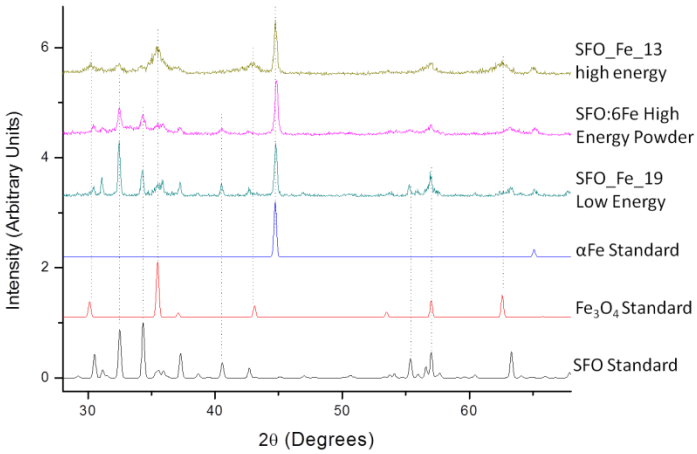

Figure 3.3.5.1 XRD profile of low energy milled densified composite sample (SFO_Fe_19), high energy pre-densified powder and high energy milled densified composite sample (SFO_Fe_13), showing reaction in the high energy milled densified composite sample

3.4 High Pressure Tungsten Carbide Plunger System

Due to temperature limitations, higher pressure needed to be used in order to densify magnetic samples. Tungsten Carbide (WC) plungers were used instead of graphite ones, see **Section 2.2.2**. It was important to confirm that composition results did not change due to the replacement of graphite plungers with WC ones, as well as using higher pressure. **Figure 3.4.2** displays an XRD profile comparing compositions of densified samples at elevated pressure, and with the use of graphite and WC plungers.

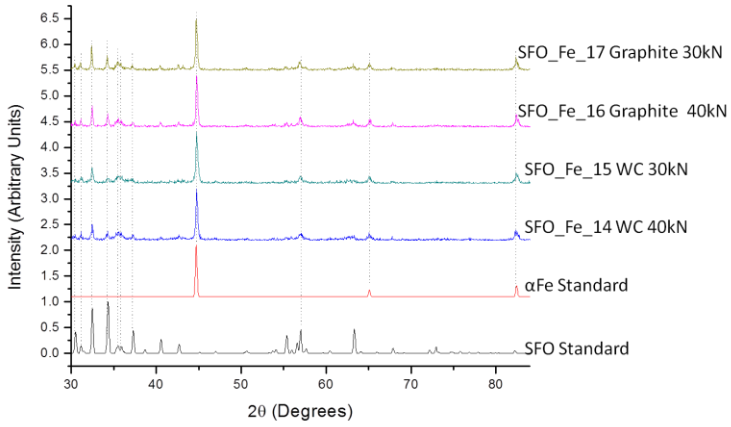

Figure 3.4.1 XRD profile showing similar composition of densified composite samples processed with WC and graphite plungers at standard (104MPa) as well as elevated (140MPa) pressures

3.5 Magnetic Properties of SFO - Micro-Fe

Magnetic data of bulk densified samples of SFO - Fe composites was collected using the VSM. The effects of Fe on SFO, composite sample density effects on magnetic properties as well as high energy ball milling effects on magnetic properties were investigated.

3.5.1 Effect of Fe in the SFO - 3Fe composite

Figure 3.5.1.1 shows a hysteresis loop comparing densified SFO sample (SFO_1) and a densified SFO - 3Fe composite sample (SFO_Fe_12). Higher magnetization saturation but lower remanence and energy product are observed in the composite material.

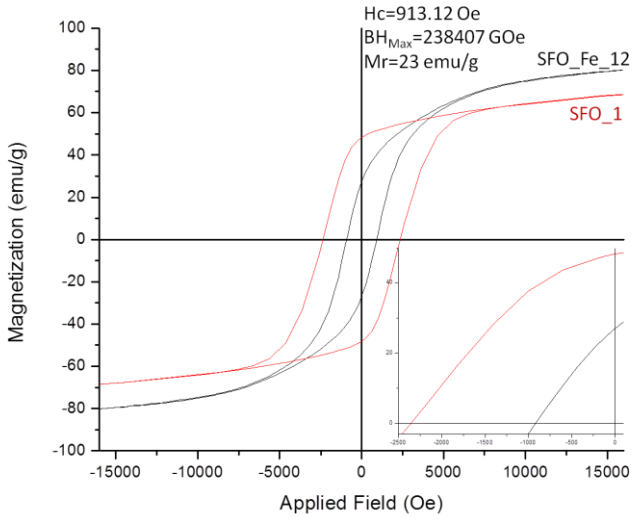

Figure 3.5.1.1 Hysteresis curve showing the effect of Fe on magnetic properties of SFO - 3Fe densified composite sample; increased magnetic saturation but decreased remanence and coercivity of densified composite sample (SFO_Fe_12) are observed when comparing to a densified SFO sample (SFO_1)

3.5.2 Effect of Processing Pressure on Density and Magnetic Properties of SFO - 6Fe Composite

Various tooling was used to increase CAPAD processing pressure in order to achieve higher densified composite sample density. Density plays a crucial role on most material properties, and magnetism is no exception. **Figure 3.5.2.1** shows a hysteresis curve comparing two densified samples of 1 mol SFO to 6 mol Fe composition. Both samples were processed at 500^{o}C. One densified composite sample was processed at 140MPa (SFO_Fe_5) and the other at 300MPa (SFO_Fe_19). The sample with higher densification pressure shows higher relative density, 74% vs. 66%, as well as larger coercivity, remanence, saturation magnetization and energy product.

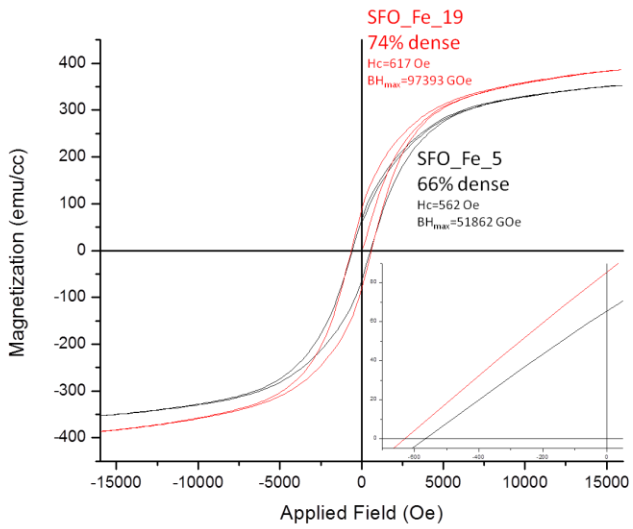

Figure 3.5.2.1 Hysteresis curve showing a positive effect of processing pressure on magnetic properties of densified SFO - 6Fe composite samples (SFO_Fe_5) and (SFO_Fe_19); increased coercivity, remanence and saturation magnetization are observed with an increase in processing pressure

3.5.3 Effect of High Energy Milling on SFO - 3Fe Composite Magnetic Properties

Figure 3.5.3.1 displays a hysteresis loop showing a comparison between densified samples of SFO as well as densified composite samples prepared from low energy and high energy milled powders as described in **Section 2.1.2** and **Section 2.1.3**. Planetary ball milling shows a negative effect on magnetic properties of CAPAD densified SFO - 3Fe composite sample (SFO_Fe_20). A reduction in coercivity, remanence and energy product is observed, when compared to pure densified SFO (SFO_1) and densified composite sample prepared from low energy powder (SFO_Fe_18).

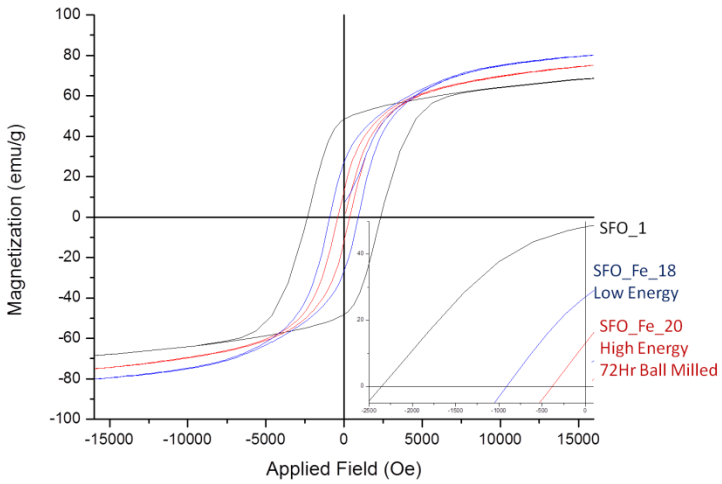

Figure 3.5.3.1 Hysteresis curve showing the effect of high energy milling on magnetic properties of SFO - 3Fe densified sample (SFO_Fe_20); poor magnetic properties are observed when comparing to densified SFO (SFO_1) as well as densified composite sample prepared from low energy milled powder (SFO_Fe_18)

3.6 Effect of Densification Temperature on Density of the SFO - 6Fe System

Data on relative density of CAPAD processed samples versus processing temperature was collected. Processing temperature was altered in order to study the effect of processing temperature on the relative density of 1 mol SFO to 6 mol Fe composite samples. Increase in processing temperature yield an increase in density to above 90% relative density (assuming desired composition). **Figure 3.6.1** shows a summary of processing temperature vs. relative density findings. Relative density increases readily with increasing densification temperature. Processing pressure was held constant at 104 MPa.

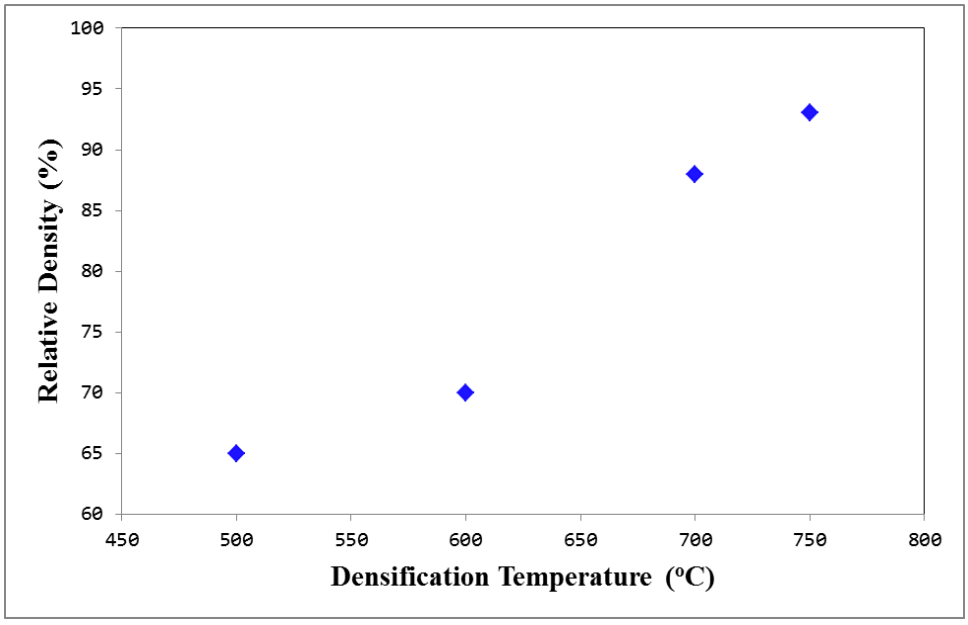

Figure 3.6.1 Relationship between densification temperature and relative density (assuming desired composition) of SFO - 6Fe composite system, showing an increase in relative density at with higher densification temperature

3.7 Effect of Densification Pressure on Density of the SFO - 6Fe system

Processing Pressure was altered in order to study its effect on the relative density of 1 mol SFO to 6 mol Fe CAPAD processed composite samples. Different types of tooling were used in order to achieve high processing pressures. Tungsten carbide plungers, as discussed in **Section 2.2.2** were introduced to achieve processing pressures 140MPa to 250MPa. **Figure 3.6.2** shows a preliminary summary of processing pressure vs. relative density findings. An increase of 5% in relative density is observed by using tungsten carbide plungers at 250MPa, when compared to using graphite plungers at 104MPa. Processing temperature was held constant at 500^{o}C.

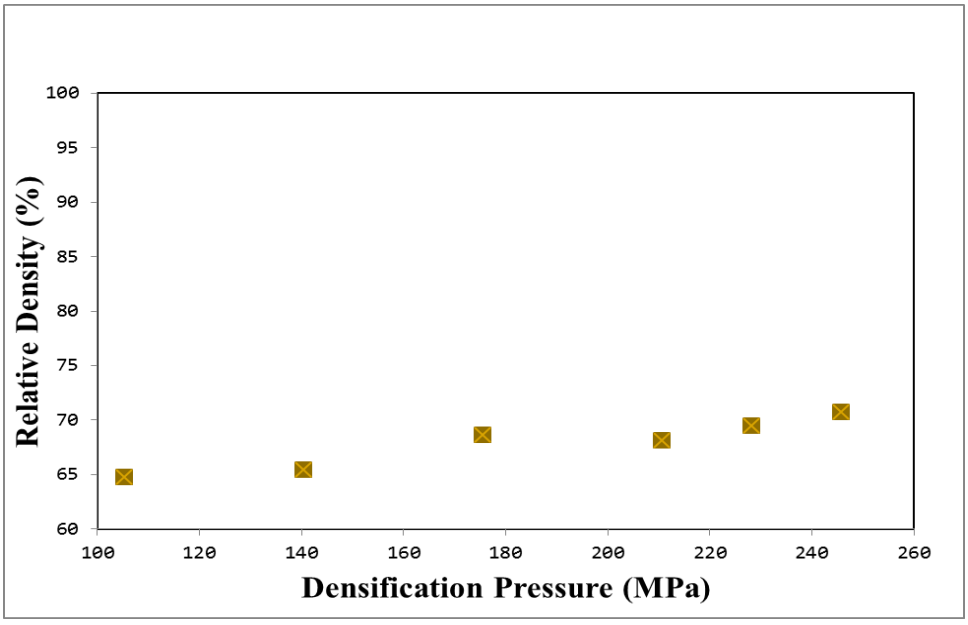

Figure 3.6.2 Relationship between densification pressure and relative density of the SFO - 6Fe composite system, showing an increase in relative density at higher processing pressures; tungsten carbide plungers were used at pressures above 104 MPa

Processing Pressure was further increased using the mini system, discussed in **Section 2.2.2,** in order to increase density to above 90%. **Figure 3.6.3** shows a complete summary of processing pressure vs. relative density findings for 1 mol SFO to 6 mol Fe composite samples. Different color data points correspond to different tooling used to achieve high processing pressures. The green data point at 104MPa was attained using the graphite plunger set-up, discussed in **Section 2.2.1**, the yellow data points at 140MPa to 250MPa were attained by replacing graphite plungers with tungsten carbide ones, discussed in **Section 2.2.2**, the blue data points at 300MPa to 450MPa were attained by using the mini tungsten carbide system, discussed in **Section 2.2.2**, and the black data point at 560MPa was attained using the mini tungsten carbide system and running the CAPAD twice on the same sample. Processing temperature was held constant at 500^{o}C.

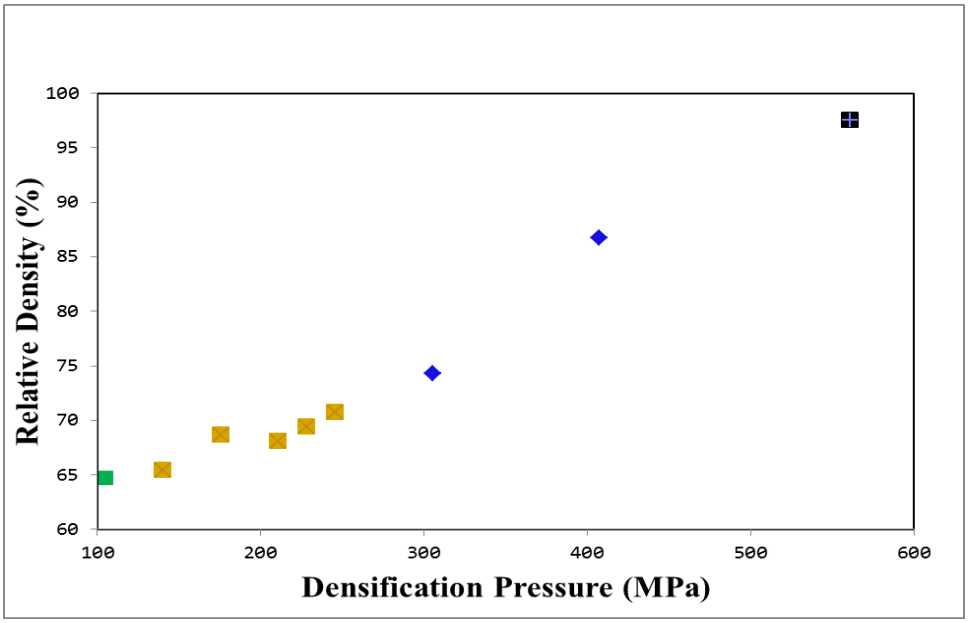

Figure 3.6.3 Relationship between densification pressure and relative sample density of the SFO - 6Fe composite system, showing much higher relative density with increased densification pressure; different colors correspond to different tooling used to achieve high densification pressure

Chapter 4 Discussion

4.1 SFO

Thanks to SFO's high magnetic anisotropy, K~3.3x10^6 erg/cc [21], it is excellent to use as a hard phase in a composite permanent magnet. Magnetic properties of CAPAD processed SFO, shown in **Figure 3.1.1.7**, confirm that high coercivity of 2400 Oe could be achieved by consolidating as received commercial powder in the CAPAD. The single domain size of SFO is ~500nm [22]. SFO starting powder micrographs, **Figures 3.1.1.1-3.1.1.5,** show that the starting powder is only slightly larger than the single domain size, making this particular powder an excellent choice as a hard phase for the hard - soft composite. The BH_{max} of 1.02 MGOe could be improved upon by increasing the magnetic saturation and remanence of this material through exchange coupling with a soft magnetic material.

4.2 SFO - γFe_2O_3

The first magnetically soft material tired in composite study was γFe_2O_3 because of its abundance, well studied properties and low price. γFe_2O_3 was mixed with SFO in mol ratios of 1 mol SFO to 1 mol γFe_2O_3,1 mol SFO to 2 mol γFe_2O_3, and 1 mol SFO to 3 mol γFe_2O_3. γFe_2O_3 has a theoretical saturation magnetization of 87.7 emu/g, which is higher than SFO's theoretical saturation magnetization of 75.6 emu/g [13]. γFe_2O_3 coupled together with SFO should have a higher magnetic response, hence yielding a higher remanence, saturation magnetization and overall energy product.

The results of the SFO - γFe_2O_3 material system study are not as promising as were hoped for. **Figure 3.2.1** shows the comparison between hysteresis curves of SFO densified sample, SFO_1, and three densified samples of 1:1 (SFO_Fe_2O_3_1), 1:2 (SFO_Fe_2O_3_2) and 1:3 (SFO_Fe_2O_3_1) mol SFO to mol γFe_2O_3 compositions. Judging from the hysteresis curve in the second quadrant, the coercivity, remanence and the energy product (larges rectangular area under the hysteresis curve) have all diminished with the addition of more γFe_2O_3. The positive aspect of these results show that the reduction of magnetic properties is not as substantial as dictated by the rules of mixtures, SFO_Fe_2O_3_3 does not have 1/3 the magnetic properties of SFO_Fe_2O_3_1. As seen with SFO_Fe_2O_3_3, the magnetic saturation is slightly larger than that of the pure densified SFO sample (SFO_1), meeting the increased magnetic saturation goal of the study. It is apparent that the slight difference between the theoretical saturation magnetization of SFO and γFe_2O_3 is not enough to increase the magnetic saturation, remanence and energy product substantially. A different soft magnetic material with a much higher magnetic saturation is required for the task.

4.3 αFe

αFe is a widely available material with a very high theoretical magnetic saturation of 245 emu/g [14]. Compared to γFe_2O_3's 87.7 emu/g, αFe's 245 emu/g should be more than double as effective in increasing the magnetic saturation, remanence and energy product of the magnetic composite. If coupled well with SFO, the SFO - Fe composite

should have a much higher remanence, saturation and energy product, compared to the unmodified SFO material.

Nano-Fe powder with a reported particulate size of 25nm was the first Fe candidate for as a soft magnetic material. Starting powder SEM micrographs, seen in **Figures 3.1.2.1-3.1.2.4,** reveal that the particulates are in fact on the nano-scale; however they are heavily agglomerated, with some particles as large as 50 microns. The powder is reported as partially passivated. Unfortunately, the XRD profile in **Figure 3.1.2.5** reveals that a sample densified from this powder (NanoFe_1) has more FeO than αFe, judging by the relative intensities of the XRD profile peaks. The magnetic properties of the same NanoFe_1 sample have been measured using the SQUID. The hysteresis curve in **Figure 3.1.2.6** reveals that in comparison to densified SFO (SFO_1), NanoFe_1 has a much lower saturation magnetization, because the majority of the sample's composition, FeO, behaves as a paramagnet at room temperature. This finding confirms that the Nano-Fe is not useful as a soft magnetic material in the composite.

The problem with buying nano Fe is that it generally comes passivated, and since the particulates are so small, the oxidized surface layer is a major part of the volume, so most of the powder is an oxide. A top down approach, involving breaking down large, commercially bought Fe particulates, was chosen in order to have more pure Fe in the system. Larger particles have less volume fraction of oxidized Fe, since the interior of the particle is much larger than the oxidized surface. The problem lies with the fact that through the use of large particles, desired level of exchange coupling with SFO will not be possible, since there is less relative Fe particulate surface area to be in contact with

SFO. With the use of a high energy planetary ball mill, as discussed in **Section 2.1.3**, particles could be milled down to smaller particulate size, with increased surface area; and become well mixed with SFO, resulting in large interfacial area that amplifies the effects of exchange coupling.

4.4 SFO - αFe

Since passivated nano powder will always have a large volume fraction of oxidized material, due to the high surface to inner volume ratio for nano material, the top down approach, as discussed in **Section 4.3**, was chosen. Another αFe powder was purchased with an average particulate size of <10 microns (Micro-Fe). Micro-Fe starting powder SEM micrographs seen in **Figures 3.1.3.1 - 3.1.3.5** show nice spherical Fe particulates with the advertised crystallite size. Starting powder, as well as a densified Fe sample (MicroFe_1) showed phase purity, as confirmed by XRD profile in **Figure 3.1.3.6**. The hysteresis curve of MicroFe_1 is shown in **Figure 3.1.3.6**. Compared to pure densified SFO (SFO_1), the saturation magnetization of MicroFe_1 is much larger, inspiring high hope for increased magnetic properties, when coupled with SFO. MicroFe_1, a 96% dense sample saturates to 96% of the theoretical Fe saturation magnetization value on a per volume basis. If coupled well, the composite made from SFO and Micro-Fe powder could show remarkable magnetic properties.

4.4.1 SFO - Fe Processing Temperature Study

In order to reach full density, samples are usually densified at temperatures around half of their melting point, in order for volume diffusion densification mechanisms to work actively. **Figure 3.6.1** shows an increase in relative sample densities (assuming desired composition) with increasing processing temperature.

As seen in **Figure 3.3.1.1**, densified 1 mol SFO to 6 mol Fe composite samples, such as SFO_Fe_4, SFO_Fe_3 and SFO_Fe_2, that were CAPAD processed at 600^{o}C and above showed no SFO or Fe in their composition. Instead, FeO and another composition of the Strontium Ferrite is present. As seen in the Strontium-Oxide and Iron-Oxide material system phase diagram, **Figure 4.4.1.2,** there is more than one composition of SrO and Fe-O. With the addition of extra Fe in the composite system, $SrFe_{12}O_{19}$ hexagonal SFO phase reacts to form the orthorhombic $Sr_4Fe_6O_{13}$ phase and Fe-O (Fe_3O_4 at lower temperature and FeO at higher temperature). $Sr_4Fe_6O_{13}$ phase, with a lower Fe-O content than $SrFe_{12}O_{19}$, is seen in the phase diagram. A phase with a lower Fe-O content is expected, since we see Fe-O as one of the products in the SFO - Fe reaction, and the diffusion of oxygen from SFO to highly reactive Fe is very plausible.

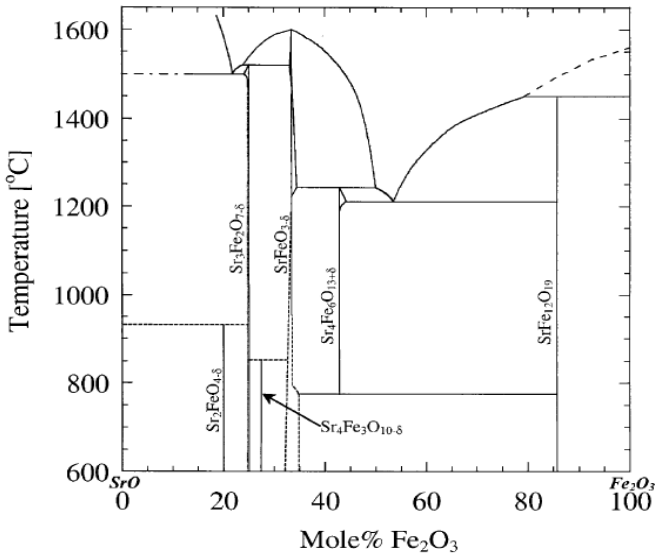

Figure 4.4.1.1 SrO - Fe_2O_3 phase diagram [23]

Densified sample SFO_Fe_1, with processing temperature of 500°C shows SFO and αFe present in its composition. Because of the limitation in temperature to 500°C, however, relative density of only 65% was achieved. The amount of densification in the CAPAD could be increased with several parameters. Higher processing temperature, higher processing pressure and longer hold time at temperature produce higher sample densities. Densified samples SFO_Fe_5, SFO_Fe_6 and SFO_Fe_7 with relative densities of 66%, 67% and 71% respectively, show the effects of higher pressure, longer hold time and higher temperature, respectively. XRD profile in **Figure 3.3.2.1** shows that modifying processing parameters slightly to increase density has no effect on composition, and the SFO and Fe phases are still present, judging from the XRD profile.

The degree of reactivity within the CAPAD of the SFO - Fe system varies slightly with starting powder composition. A study of 1 mol SFO to 12 mol Fe densified samples

reveal a higher degree of reactivity. **Figure 3.3.3.1** shows the XRD profile of densified samples SFO_Fe_8, SFO_Fe_9, SFO_Fe_10 and SFO_Fe_11. Sample SFO_Fe_8, densified at 450^{o}C shows no sign of Fe-O, and displays SFO and Fe peaks. At 500^{o}C, with sample SFO_Fe_9, we see a decrease in intensity of SFO peaks, when comparing it to SFO_Fe_8. SFO_Fe_10, densified at 550^{o}C no longer shows any SFO peaks, and is composed mostly of FeO and excess Fe. When comparing this to a SFO - 6Fe densified sample (SFO_Fe_7), processed at the same conditions as SFO_Fe_10, it is clear that the 1:12 composition is more reactive. Then thinking about the amount of reactants present, it makes sense for a powder with a higher Fe content to be more reactive, since there is more of it to react with SFO and make FeO. While the XRD profile of 1:6 mol ratio samples show diminishing intensity of Fe peaks with an increase in temperature, 1:12 mol ratio samples display consistent Fe peak intensity, signifying that there is a lot of excess Fe reactant left. The high reactivity of the powders at elevated temperatures limits the temperature range to about 500^{o}C, which is not enough to achieve high density.

4.4.2 Increasing the Density of SFO - Fe Using Tungsten Carbide (WC) Plungers

In order to produce higher density samples with the CAPAD process, higher temperature, longer hold times and higher pressures must be applied. The SFO - Fe system reacts to unwanted products at higher temperatures, so the limit of temperature is set around 500^{o}C. Longer hold time gives only a slight increase in relative density, as observed by comparing densified samples SFO_Fe_1's 65% to SFO_Fe_6's 67% relative density. An increase in relative density of 2% is observed with a 5 minute hold time. The

negative effect of holding the densified sample at processing temperature is increased grain growth. SFO - Fe composite samples are limited in densification temperature to a relatively low 500^{o}C. Increased duration of time spent at low temperature promotes sintering, surface diffusion and grain growth more than volume diffusion and densification, when compared to samples densified at higher temperatures. As mentioned in **Section 1.3 Coercivity Dependence on Particle Size**, it is important to keep grains small in order to achieve the best coercivity possible in the composite magnet. Smaller grains also contribute to an increased effect of exchange coupling, since smaller grains have larger relative surface area to be shared as interfacial area between soft and hard phases. This leaves the increase in densification pressure the only viable option to achieve higher sample density and keep small grains and desired composition. Densified sample SFO_Fe_5, processed at 140MPa only showed an increase in relative density of 1% over SFO_Fe_1, which was processed at 104MPa. It is obvious that a much higher densification pressure is required to attain high degree of densification with the CAPAD process.

The typical CAPAD set up involves the use of two graphite plungers to apply pressure to the powder and transfer current to the die and powder, as discussed in **Section 1.6**. The compressive strength of high quality graphite is about 140MPa. This limits the densification pressure of the process if graphite plungers continue to be used. A replacement material is necessary in order to create a high pressure system. The new plungers must be made of a high compressive strength material which is also a good electrical conductor. Tungsten Carbide (WC) fits the role of a graphite replacement well

with its high electric conductivity and a compressive strength of up to 4GPa [24], see **Figure 2.2.2.1**. Effects of pressures from 104 MPa to 250 MPa where studied on 1 mol SFO to 6 mol Fe composite system densified at 500^{o}C with no hold time. As seen in **Figure 3.6.2**, increase in processing pressure has an increasing effect on relative density; however, the highest pressure available due to stainless puck creep failure limitations is only enough to achieve a 5% relative increase in density, as compared to 104MPa graphite plunger set-up.

As discussed in **Section 2.2.2**, because of the load limitations in place, due to the lack of compressive strength at high temperature of stainless steel, a reduction in sample area route was chosen to increase densification pressure. As seen in **Figure 2.2.2.2,** a mini die and plunger system with the inner diameter of 9.5mm is placed inside the 19mm die and plunger system. WC plungers are used for both the outer and inner systems. Because of the reduction in area, much higher pressures can be achieved. A summary of density findings is displayed in **Figure 3.6.3**. One can see much higher densities achieved with the mini high pressure system.

4.5 Microstructure Analysis

In order to have good exchange coupling within the composite magnet, the hard and soft phases must be well intermixed with each other. Maximizing the contact surface area between the two phases is critical for magnetic properties of an exchange coupled magnet. **Figures 3.3.4.1 - 3.3.4.6** show SEM micrographs of densified sample SFO_Fe_12 made with low energy milled powder. It is obvious from the micrographs

that the Fe distribution within the microstructure of SFO_Fe_12 is very broad. **Figure 3.3.4.6** however, shows good interphase between Fe and SFO. Based on contrast difference, there is a clear line seen in the micrographs, where Fe ends and SFO begins. Even though there appears to be good interphase between SFO and Fe, there is not enough of it.

A reduction of grain size and better distribution of Fe within the composite would greatly increase the surface area shared between the hard and soft phases. Fritsch Planetary Micro Mill Pulverisette 7 Premium Line planetary high energy ball mill was used to mill Fe and SFO particulates together, as discussed in **Section 2.1.3**. XRD profiles in **Figure 3.3.5.1** reveal that the powder after the high energy ball milling process is not reacted, and displays the same peaks as a low energy milled densified composite sample (SFO_Fe_19). However, after CAPAD processing of the high energy milled powder, reaction occurs at a lower temperature than expected. It is possible that the extra surface area, as well as the extra kinetic energy given to the powder during the high energy milling process, combined with the thermal energy given to the powder in the CAPAD is enough for reaction to occur, even at 500^{o}C. The resulting sample's (SFO_Fe_13) XRD profile displays cubic Fe-O peaks.

4.6 Magnetic Results of the SFO - Fe Composite

Magnetic data for the SFO - Fe composite system has been collected using the lakeshore VSM. One of the main goals for this study has been to increase the magnetic response of the hard SFO phase to achieve higher saturation magnetization and

remanence, with the addition of the soft Fe phase. **Figure 3.5.1.1** depicts a hysteresis loop of densified SFO - 3Fe composite sample (SFO_Fe_12) compared to densified SFO (SFO_1). There is an increase in saturation magnetization of the composite material, when compared to the hard phase alone, meeting one of the goals of the study. As expected, the composite densified sample has a lower coercivity, due to a higher volume fraction of the soft phase. Unfortunately, the composite material has lower remanence, indicating a low degree of coupling between the hard SFO and the soft Fe phases. The extra magnetic moment added to the composite by the soft Fe phase increases the saturation magnetization but does not result in a higher remanence. If however the SFO and Fe were coupled, the SFO would keep Fe's moments aligned even if no external magnetic field is applied, and a high remanence value would have been present. Overall, the BH_{max} of the densified composite (SFO_Fe_12) is about a fourth of densified SFO (SFO_1). It is not surprising that a low degree of coupling is present within the composite; as we've seen in **Figure 3.3.4.1**, the microstructure of the densified composite is not adequate for good coupling. The Fe grain size is too large and the hard SFO and soft Fe phases are not well dispersed within the composite. There is no way to achieve a significant coupling effect with <10 micron size Fe grains because there is not enough interfacial area between SFO and Fe. Interfacial area could be increased with small grains size.

Planetary ball milling was used in an attempt to tailor the microstructure of the SFO - Fe composites, as discussed in **Section 2.1.3**. Using the high energy planetary ball milling could decreases average particulate size and increase the surface to surface area

shared by SFO and Fe particulates. Hysteresis curve in **Figure 3.5.3.1** shows a comparison between densified SFO (SFO_1), low energy milled powder densified composite sample (SFO_Fe_18) and high energy milled powder densified composite sample (SFO_Fe_20). SFO_Fe_20 shows much worse magnetic properties than SFO_Fe_18. This is unexpected since the high energy planetary ball milling should increase the surface area of hard and soft phase interaction. Thinking about the 72 hour powder milling time, it is clear that the extra energy in the powder caused a reaction within the sample, as seen in the XRD profile of **Figure 3.3.5.1**. The hard SFO phase has reacted with the soft Fe phase to form $Sr_4Fe_6O_{13}$ and cubic Fe-O, reducing all magnetic properties. Shorter milling times will be investigated in the future.

Density plays an important role in magnetic properties. A sample with a lot of pores will have poor magnetic properties, since trapper air or vacuum in pores has virtually no magnetic contribution. More magnetic material packed in a volume will have a higher magnetic response. This is demonstrated in **Figure 3.5.2.1**. Sample SFO_Fe_19 and SFO_Fe_5 were processed at the same CAPAD conditions, save the densification pressure. SFO_Fe_19 is 74% dense while SFO_Fe_6 is 66% dense. On a per volume basis, SFO_Fe_19 exhibits higher coercivity, remanence, saturation magnetization and BH_{max}. A 12% relative increase in density gives a non linear 31% relative increase in remanence, 10% relative increase in coercivity and 88% relative increase in BH_{max}. A large increase in magnetic properties, compared to a relatively small increase in density is revealed. By increasing densification pressure, through the use of non-traditional tungsten carbide tooling, as discussed in **Section 2.2.2**; increasing relative composite sample

density, while preserving the desired composition within the composite material has been observed. Benefits of higher processing pressure on the magnetic properties of the SFO - Fe composite are immense.

4.7 Conclusion

In conclusion, a study on producing hard - soft magnetic composites using CAPAD has brought about some interesting preliminary results. First, the addition of γFe_2O_3 as a soft phase material in a SFO - γFe_2O_3 composite did not contribute enough moment to increase magnetic properties, and instead diluted SFO's remanence and coercivity. Nano sized Fe was passivated and its magnetic saturation did not surpass that of pure SFO, yielding Nano-Fe useless for the exchange coupled hard - soft composite magnet. Micron sized Fe has only a small layer of passivation, and is mostly pure Fe on a per volume basis. Samples made with SFO and micro-Fe exhibit a higher saturation magnetization than pure SFO samples, meeting one of the requirements of the composite magnet. However, remanence and coercivity are lower than unmodified SFO. Non-ideal microstructure and lack of coupling is to blame for poor remanence, coercivity and energy product of the composite. The microstructure of densified samples made with low energy tumble milled powder display lack of good Fe dispersion within the composite. The Fe grains are also too big to provide enough interfacial area for good coupling. The powders mixed with the high energy ball milling displayed worse magnetic properties due to reaction in the CAPAD. Non-traditional tungsten carbide tooling for high densification pressure CAPAD processing was shown to increase relative density of

composite samples, while keeping desired composition. An increase in relative density was shown to have a positive effect on magnetic properties. A 12% relative increase in density boosted the energy product by 88%.

References:

[1] Milmo, Cahal. "Concern as China Clamps down on Rare Earth Exports." The Independent. Independent Digital News and Media, 02 Jan. 2010. 2 Apr. 2012. <http://www.independent.co.uk/news/world/asia/concern-as-china-clamps-down-on-rare-earth-exports-1855387.html>.

[2] "Neodymium Iron Boron Magnets - General Information." Neodymium Iron Boron Magnets. 02 Oct. 2011. <http://www.rare-earth-magnets.com/?gclid=CLWaoLP1-bECFUpxQgodDwMAHA>.

[3] Nave, R. "Magnetic Potential Energy." Magnetic Potential Energy. 28 June 2012. <http://hyperphysics.phy-astr.gsu.edu/hbase/magnetic/magpot.html>.

[4] R. Coehoorn, D.B. Mooji, C. DeWaard. Journal of Magnetism and Magnetic Materials, 80 (1989) 101.

[5] R. Fischer, T. Schrefl, H. Kronmuller, and J. Fidler. "Grain-size Dependence of Remanence and Coercive Field of Isotropic Nanocrystalline Composite Permanent Magnets." Journal of Magnetism and Magnetic Materials, 153 (1996): 35-49.

[6] Fischer, R. "Phase Distribution and Computed Magnetic Properties of High-remanent Composite Magnets." Journal of Magnetism and Magnetic Materials, 150 (1995): 329-44.

[7] M. Wilcox, J. Williams, M. Lenowicz, A. Manaf and H. Davies. 8th International Symposium on Magnetic Anisotropy and Coercivity in Rare-earth Transition Metal Alloys, Birmingham. Sept 15, 1994.

[8] Sun, X. K., Jian Zhang, Yelong Chu, Wei Liu, Baozhi Cui, and Zhidong Zhang. "Dependence of Magnetic Properties on Grain Size of α-Fe in Nanocomposite $(Nd,Dy)(Fe,Co,Nb,B)_{5.5}$/α-Fe Magnets." Applied Physics Letters 74.12 (1999): 1740.

[9] Zeng, Hao, Jing Li, J. P. Liu, Zhong L. Wang, and Shouheng Sun. "Exchange-coupled Nanocomposite Magnets by Nanoparticle Self-assembly." Nature 420.6914 (2002): 395-98.

[10] Chikazumi, Sōshin, C. D. Graham, and Sōshin Chikazumi. Physics of Ferromagnetism. Oxford: Clarendon, 1997.

[11] Goldman, Alex. Modern Ferrite Technology. New York: Springer, 2006. Print.

[12] Ding, J. "High Coercivity Ba Hexaferrite Prepared by Mechanical Alloying." Journal of Alloys and Compounds 221.1-2 (1995): 70-73.

[13] Liu, Xiansong, Wei Zhong, Benxi Gu, and Youwei Du. "Exchange-coupling Interaction in Nanocomposite $SrFe_{12}O_{19}/\gamma$-Fe_2O_3Permanent Ferrites."*Journal of Applied Physics* 92.2 (2002): 1028.

[14] Danan, H. A., and J. P. Meyer. "New Determinations of the Saturation Magnetization of Nickel and Iron." Journal of Applied Physics. 1 Feb. 1968.

[15] Moskowitz, Bruce. "Domain Theory." *Hitchhiker's Guide to Magnetism*. 5 June 1991. <http://www.irm.umn.edu/hg2m/hg2m_d/hg2m_d.html>.

[16] "History of Sintering." CISP History. Center for Innovative Sintered Products, n.d. Web. 17 July 2012. <http://www.cisp.psu.edu/history_sintering.html>.

[17] Kingery, W. David; Bowen, H. K.; Uhlmann, Donald R. (April 1976). Introduction to Ceramics (2nd ed.). John Wiley & Sons, Academic Press.

[18] The Zang Research Group, <http://www.eng.utah.edu/~lzang/images/lecture-9-Ostwald-ripening-particle-coarsening-lecture.pdf>.

[19] Garay, J.E. "Current-Activated, Pressure-Assisted Densification of Materials." Annual Review of Materials Research 40.1 (2010): 445-68.

[20] "Inorganic Crystal Structure Database." Web. <http://www.fiz-karlsruhe.de/icsd.html>.

[21] Wohlfarth, E. P., and K. H. J. Buschow. Ferromagnetic Materials: A Handbook on the Properties of Magnetically Ordered Substances. Amsterdam: North-Holland Pub. 1980.

[22] Nawathey-Dikshit, Rashmi, S. R. Shinde, S. B. Ogale, S. D. Kulkarni, S. R. Sainkar, and S. K. Date. "Synthesis of Single Domain Strontium Ferrite Powder by Pulsed Laser Ablation." Applied Physics Letters 68.24 (1996): 3491.

[23] Fossdal, Anita, Mari-Ann Einarsrud, and Tor Grande. "Phase Equilibria in the Pseudo-binary System SrO–Fe2O3." Journal of Solid State Chemistry 177.8 (2004): 2933-942.

[24] "Tungsten Carbide Information - Provided by Insaco Inc" <http://www.insaco.com/MatPages/mat_display.asp?M=TC>.